Timing of detachment faulting in the Bullfrog Hills and Bare Mountain area, southwest Nevada: Inferences from ^{40}Ar/^{39}Ar, K-Ar, U-Pb, and fission track thermochronology

Thomas D. Hoisch

Department of Geology, Northern Arizona University, Flagstaff

Matthew T. Heizler

New Mexico Bureau of Mines and Mineral Resources, New Mexico Institute of Mining and Technology, Soccoro

Robert E. Zartman[1]

U.S. Geological Survey, Denver, Colorado

Abstract. Crustal extension in the Bullfrog Hills and Bare Mountain area of southwest Nevada is associated with movement along a regional detachment fault. Normal faulting in the upper plate and rapid cooling (denudation) of the lower plate were coeval with Miocene silicic volcanism and with west-northwest transport along the detachment fault. A west-northwest progression of tilting along upper plate normal faults is indicated by ages of the volcanic rocks in relation to angular unconformities. Near the breakaway, tilting in the upper plate occurred between 12.7 and 11.6 Ma, continued less strongly past 10.7 Ma, and was over by 8.2 Ma. Ten to 20 km west of the breakaway, tilting occurred between 10.7 and 10.33 Ma, continued less strongly after 10.33 Ma, and was over by 8.1 Ma. The cooling histories of the lower plate metamorphic rocks were determined by thermochronologic dating methods: K-Ar and ^{40}Ar/^{39}Ar on muscovite, biotite, and hornblende, ^{40}Ar/^{39}Ar on K-feldspar, U-Pb on apatite, zircon, and sphene, and fission track on apatite, zircon, and sphene. Lower plate rocks 10 km west of the breakaway cooled slowly from Early Cretaceous lower-amphibolite facies conditions through 350±50° to 300±50°C between 57 and 38 Ma, then cooled rapidly from 205±50° to 120±50°C between 12.6±1.6 and 11.1±1.9 Ma. Lower plate rocks 20 km west of the breakaway cooled slowly from Early Cretaceous upper-amphibolite facies conditions through 500±50°C at 78-67 Ma, passed through 350±50° to 300±50°C between 16.3±0.4 and 10.5±0.3 Ma, then cooled rapidly from 285±50° to 120±50°C between 10.2 and 8.6 Ma. Upper plate tilting and rapid cooling (denudation) of the lower plate occurred simultaneously in the respective areas. The early slow-cooling part of the lower plate thermal histories was probably related to erosion at the Earth's surface, which stripped off about 9 km of material in 50 to 100 m.y. The results indicate an initial fault dip ≥30° and a 12 mm yr^{-1} west-northwest migration of the locus of rapid tilting in the upper plate.

Introduction

Many studies have documented regional detachment (low-angle normal) faults in areas of large-magnitude crustal extension [e.g., *Crittenden et al.*, 1980; *Davis and Coney*, 1979]. The lower plate typically consists of mylonitic plutonic and metamorphic rocks that were rapidly denuded while the faults were active. Theories have been proposed to explain how detachment faults, which are presently horizontal or dip gently (<15°) at the Earth's surface, accommodated the denudation of middle or lower crustal rocks. A number of studies [*Buck*, 1988; *Hamilton*, 1988a,b; *Spencer and Reynolds*, 1991; *Wernicke and Axen*, 1988] have suggested a rolling hinge model, in which movement occurs

along a dipping fault segment that progressively rotates to a subhorizontal orientation; the rotated segment becomes inactive while the dipping segment migrates in the direction of upper plate transport. Tilting of the lower plate rocks associated with the rotation of detachment faults has been inferred in field studies [*Axen*, 1993; *Axen et al.*, 1995; *Bartley et al.*, 1990; *Coleman and Walker*, 1994; *Hoisch and Simpson*, 1993; *Holm and Wernicke*, 1992; *Manning and Bartley*, 1994; *McGrew and Snee*, 1994; *Miller*, 1991; *Selverstone et al.*, 1995; *Spencer and Reynolds*, 1989] and modeled in theoretical or analog studies [*Brun et al.*, 1994; *Buck*, 1993; *King and Ellis*, 1990; *Melosh*, 1990; *Wdowinski and Axen*, 1992]. The progressive unroofing of the lower plate is confirmed by thermochronologic studies in which cooling ages become younger in the direction of upper plate transport [*Hoisch and Simpson*, 1993; *Holm and Dokka*, 1993; *Holm et al.*, 1992; *Foster et al.*, 1993; *Lee*, 1995; *John and Foster*, 1993; *McGrew and Snee*, 1994].

Different studies have reached different conclusions concerning the dip angle of the fault at the time of movement. Moderate angles (30-60°) have been inferred in some studies [*Davis*, 1983,

---

[1]Now at Department of Geological Sciences, University of Cape Town, Rondebosch, Republic of South Africa
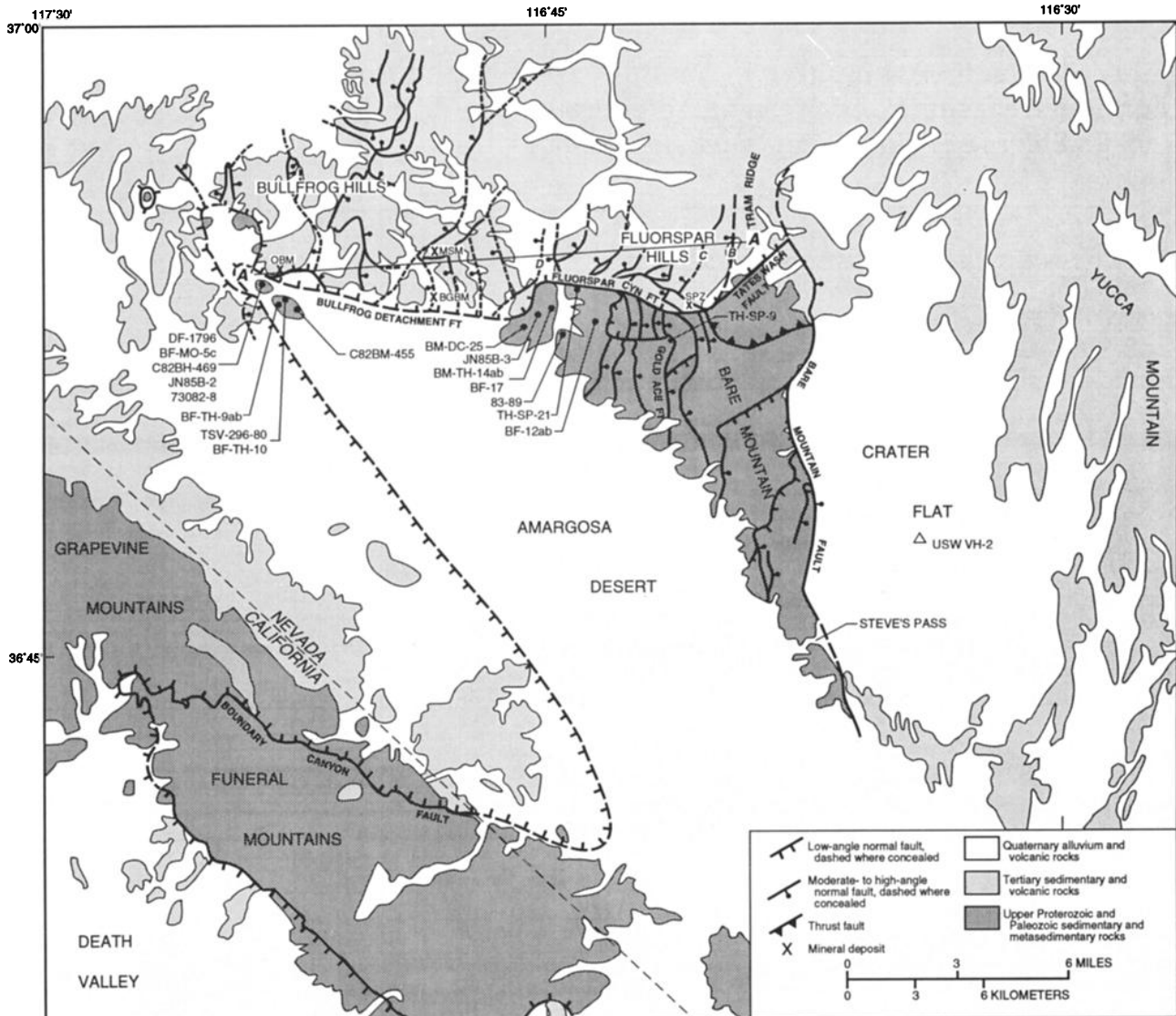
Figure 1. General geology of the study area, locations of all features mentioned in the text, and locations of thermochronology samples. Major upper plate normal faults in the Fluorspar Hills and Bullfrog Hills, and major normal faults in the lower plate at Bare Mountain are shown. Transect A-A' and faults labeled B, C, and D are referred to in Figure 8. OBM, Original Bullfrog Mine; BGBM, Barrick Gold Bullfrog Mine; MSM, Montgomery-Shoshone Mine; SPZ, Secret Pass zone of mineralization. Geology based on work by *Cornwall and Kleinhampl* [1961], *Frizzell and Shulters* [1990], *Maldonado* [1990a], *Maldonado and Hausback* [1990], *Monsen et al.* [1992], *Wright and Troxel* [1993], and M.D. Carr (U.S. Geological Survey, unpublished map, 1994).

1987; *Hoisch and Simpson*, 1995; *McGrew and Snee*, 1994; *Lee*, 1995; *Richard et al.*, 1990] and dips less than 30° have been inferred in other studies [*Axen*, 1993; *John and Foster*, 1993; *Livacarri et al.*, 1993, 1995; *Davis and Lister*, 1988; *Miller and John*, 1988; *Scott and Lister*, 1992; *Wernicke et al.*, 1984; *Yin and Dunn*, 1992]. A moderate angle is consistent with earthquake focal mechanisms which indicate that most, if not all, active extension occurs along moderately dipping normal faults [*Jackson*, 1987]. Several mechanisms have been proposed to overcome problems with the initiation and propagation of low-angle normal faults [*Axen*, 1992; *Axen and Selverstone*, 1994; *Brun et al.*, 1994; *Melosh*, 1990; *Spencer and Chase*, 1989; *Yin*, 1989] and with the apparent paucity of low-angle normal earthquake focal mechanisms [*Wernicke*, 1995].

This study investigated a detachment fault exposed in south-

west Nevada at Bare Mountain, in the Bullfrog Hills, and in the Funeral Mountains (Figure 1). The fault strikes east-west along Fluorspar Canyon in the northwest part of Bare Mountain [*Carr and Monsen*, 1988] and along the southern part of the Bullfrog Hills [*Ransome et al.*, 1910]. In the Funeral Mountains, it strikes southeast along the northeast flank and partly follows Boundary Canyon [*Reynolds et al.*, 1986]. The three fault segments were initially correlated by *Carr and Monsen* [1988].

The goal of this study was to evaluate the temporal relationship between normal faulting in the upper plate and denudation of the lower plate. In the upper plate, angular unconformities between well-dated Miocene volcanic strata and other dated relationships described in previous studies limit the age of tilting and faulting. In the lower plate, cooling histories are constructed from thermochronologic data (^{40}Ar/^{39}Ar, K-Ar, U-Pb, fission

track) generated in this and previous studies and used to infer the age of denudation. A basaltic dike which is cut by the Gold Ace fault (Figure 1) was also dated in this study in order to limit the age of movement.

Geologic Setting

The volcanic sequences in the upper plate were erupted mainly from several Miocene silicic volcanic centers located in the area north of Yucca Mountain [Byers et al., 1976; Carr et al., 1986; Sawyer et al., 1994]. In the Bullfrog Hills, this includes the regionally extensive 14.0-Ma Lithic Ridge Tuff, 13.3 Ma Bullfrog Tuff, 12.7 Ma Tiva Canyon Tuff, 11.6 Ma Rainier Mesa Tuff, and the 11.45 Ma Ammonia Tanks Tuff (Table 1), which total ~1790 m in thickness [Maldonado, 1990b]. In addition to these units, the 13.45 Ma Tram Tuff and 12.8 Ma Topopah Spring Tuff are present in the Fluorspar Hills at Bare Mountain, where they contribute an additional ~490 m to the total thickness [Monsen et al., 1992]. Most of these units are members of formations: the Crater Flat Tuff includes the Bullfrog and Tram Tuffs, the Paintbrush Tuff includes the Tiva Canyon and Topopah Spring Tuffs, and the Timber Mountain Tuff includes the Ammonia Tanks and Rainier Mesa Tuffs (Table 1). Many local volcanic units have also been identified [Maldonado, 1990b; Monsen et al., 1992), but most are minor in thickness. However, the 10.7-10.33 Ma "Tuffs and Lavas of Bullfrog Hills" (TLBH, informal name of Weiss et al. [1990]) are ~850 m thick [Maldonado, 1990b], and the 11.62 Ma rhyolite of Fluorspar Canyon attains thicknesses of over 390 m [Monsen et al., 1992]. Undated volcanic rocks that are local to the Bullfrog Hills underlie the Lithic Ridge Tuff and are ~2000 m thick [Maldonado, 1990b].

The upper plate Miocene volcanic sequences are variably tilted to the east-southeast along numerous normal faults that dip generally west-northwest [Ransome et al., 1910; Conners et al., 1995; Maldonado, 1990b; Monson et al., 1992]. The west-bounding fault along Tram Ridge, a faulted-bounded block capped by untilted Rainier Mesa Tuff in the eastern Fluorspar Hills (Figure 1), marks the eastern limit and breakaway of the detachment [Fridrich, 1997]. Tram Ridge is bounded on the east and south by splays off the Bare Mountain fault [Fridrich, 1997]; the south-bounding fault follows Tates Wash (Figure 1). Relative to lower plate rocks, the upper plate was extended to the west-northwest [Maldonado, 1990b; Monsen et al., 1992], consistent with shear indicators in lower plate mylonites in the Bullfrog Hills (T.D. Hoisch, unpublished data, 1993) and Funeral Mountains [Hoisch and Simpson, 1993]. Maldonado [1990b] interpreted upper plate relationships to indicate that normal faults sole into the detachment; drilling has confirmed this for normal faults at the Original Bullfrog and Montgomery-Shoshone Mines (Figure 1) (D.R. Boden, written communication, 1996). Carr [1990] concluded that upper plate normal faulting in the Fluorspar Hills is somewhat older than in the Bullfrog Hills, based on an angular unconformity between Timber Mountain and Paintbrush Tuffs in the Fluorspar Hills, and faulted post-Timber Mountain volcanic rocks in the Bullfrog Hills.

The Fluorspar Canyon segment of the detachment fault dips to the north at angles ranging from 25 to 40° [Fridrich, 1997]. The Bullfrog Hills segment is poorly exposed but probably also dips gently to the north. In the eastern Bullfrog Hills, the fault is deformed into a gently northwest-plunging antiform [Maldonado, 1990b] which connects to a similar antiform in the Funeral Mountains through an unexposed synform (Figure 1) [Carr and Monsen, 1988]. In the Bullfrog Hills, the attitudes of faulted panels in the upper plate [Maldonado, 1990a] suggest that it is folded about the axis of the antiform and that folding postdated movement along the detachment.

At Bare Mountain, the lower plate consists of uppermost Late Precambrian and Cambrian through Mississippian strata totaling ~7400 m in thickness [Monsen et al., 1992]. Metamorphosed strata are confined to a structural block that is bounded on the north by the detachment fault and on the east by an east dipping normal fault, the Gold Ace fault (Figure 1). The block reaches upper greenschist facies in the southern half and lower-amphibolite facies in the northern half [Hoisch, 1997]. The metamorphic grade drops discordantly across the Gold Ace fault, with subgreenschist facies rocks occurring in the hanging wall [Hoisch, 1997]. Conodont color alteration index data indicate

Table 1. Ages of Dated Volcanic Units at Bare Mountain and the Bullfrog Hills

Unit Name	Age, Ma	Source
Stonewall Flat Tuff		
Spearhead Member	7.6	Dieno et al. [1989]
Tuffs and Lavas of Bullfrog Hills (TLBH)*		
Latite overlying Rainbow Mountain sequence	10.33	Eng et al. [1996]
Rhyolite at base of Rainbow Mountain sequence	10.56	Eng et al. [1996]
Basalt underlying Rainbow Mountain sequence	10.7	Monsen et al. [1992]
Timber Mountain Tuff		
Ammonia Tanks Tuff	11.45	Sawyer et al. [1994]
Rainier Mesa Tuff	11.6	Sawyer et al. [1994]
Rhyolite of Fluorspar Canyon	11.62	C.J. Fridrich et al. (USGS written communication, 1994)
Paintbrush Tuff		
Tiva Canyon Tuff	12.7	Sawyer et al. [1994]
Topopah Spring Tuff	12.8	Sawyer et al. [1994]
Crater Flat Tuff		
Bullfrog Tuff	13.3	D.A. Sawyer (USGS written communication, 1995)
Tram Tuff	13.45	D.A. Sawyer et al. (USGS written communication, 1994)
Lithic Ridge Tuff	14.0	Sawyer et al. [1994]

Details of the volcanic stratigraphy are given by Byers et al. [1976], Carr et al. [1986], Eng et al. [1996], Maldonado [1990b], Ransome et al. [1910], and Sawyer et al. [1994].

*Informal name of Weiss et al. [1990].

that temperatures of 225° to 350°C were attained in the hanging wall [*Grow et al.*, 1994]. Rare muscovite granite dikes, similar to Late Cretaceous dikes in the northwest part of the Funeral Mountains (dated U-Pb on zircon by *Applegate et al.* [1992]), intrude the footwall.

In the Bullfrog Hills, the lower plate consists of pelitic schist and amphibolite, dated 1.7 Ga (this study, discussed later), that are abundantly injected by muscovite granite dikes similar to Late Cretaceous dikes in the Funeral Mountains. The pelitic schist contains garnet, staurolite, and kyanite [*Hoisch and Simpson*, 1993], similar to 1.7 Ga basement rocks (U-Pb on zircon, reported by *Wright and Troxel* [1993]) in the lower plate of the northwest Funeral Mountains. Tertiary volcanic and sedimentary strata in the upper plate are faulted against metamorphic rocks in the lower plate, except in one location where Tertiary strata lie depositionally upon subgreenschist Paleozoic strata in the upper plate (D.R. Boden, written communication, 1996). Fault-bounded slivers of subgreenschist Paleozoic strata occur locally between the upper and lower plates [*Maldonado*, 1990b].

The 1.7 Ga basement rocks and ~5000 m of metamorphosed Late Precambrian strata that underlie the section found at Bare Mountain [*Wright and Troxel*, 1993] are exposed in the lower plate of the Funeral Mountains. Tertiary strata lie depositionally upon lower Paleozoic strata of subgreenschist grade in the upper plate and the detachment fault is marked by a discordance in metamorphic grade [*Hoisch and Simpson*, 1993; *Labotka*, 1980]. The lower plate in the northwest part of the Funeral Mountains and the Bullfrog Hills is strongly mylonitic, in contrast to the lower plate at Bare Mountain which is non-mylonitic.

The age of the metamorphism has not been determined at Bare Mountain or in the Bullfrog Hills; however, two studies in the Funeral Mountains concluded that metamorphism peaked in approximately Early Cretaceous time [*DeWitt et al.*, 1988; *Applegate*, 1994]. Thermobarometry of schist from the northwest part of the Funeral Mountains indicates metamorphism at a depth of ~30 km [*Hoisch and Simpson*, 1993]. A depth of ~18 km was determined from schist in the footwall of the Gold Ace fault at Bare Mountain [*Hoisch*, 1997]. The depths represent the total amounts of postmetamorphism denudation in these two areas. Lower plate rocks in the Bullfrog Hills were probably also metamorphosed at ~30 km depth, by analogy with the petrologically similar 1.7 Ga basement rocks in the Funeral Mountains.

There are at least two families of normal faults within the lower plate at Bare Mountain, a set of moderately east dipping faults and a set of gently southeast dipping faults. The Bare Mountain fault, which forms the eastern range front, is a member of the east dipping set, as is the Gold Ace fault (Figure 1). Mapping by *Monsen et al.* [1992] showed that the southeast dipping faults cut or curve into the east dipping faults. They suggested that Bare Mountain is composed of rhombohedra, the edges of which are the curving joins between the two sets. If correct, then the two sets of faults are of similar age. One exception is the Bare Mountain fault (Figure 1), which cuts several of the southeast dipping faults [*Monsen et al.*, 1992].

Chronology of Extension

Age of Normal Faulting in the Fluorspar Hills and Along Tram Ridge

It is unclear exactly when movement along the breakaway of the detachment began. The absence of 12.7 Ma Tiva Canyon Tuff on Tram Ridge [*Fridrich*, 1997] suggests that it was a topographic high at 12.7 Ma, consistent with movement prior to

12.7 Ma. The same reasoning applies to the other faults that bound Tram Ridge, the Bare Mountain fault on the east, and the Tates Wash fault on the south (Figure 1).

Avalanche breccias shed from the breakaway scarp along the west side of Tram Ridge were deposited upon strongly east tilted (~45°) 12.7 Ma Tiva Canyon Tuff and overlain by the 11.62-Ma rhyolite of Fluorspar Canyon. An upward decrease in dip of the rhyolite of Fluorspar Canyon suggests deposition during tilting [*Fridrich*, 1997]. The 11.6 Ma Rainier Mesa Tuff is flat-lying on Tram Ridge and was deposited over the rhyolite of Fluorspar Canyon, breccias and fault [*Fridrich*, 1997]. Thus, faulting and tilting occurred between 12.7 Ma and 11.6 Ma.

In the central and western Fluorspar Hills, the 11.6 Ma Rainier Mesa Tuff and conformable 11.45 Ma Ammonia Tanks Tuff are tilted 25° to 45° [*Monsen et al.*, 1992]. A 10.7 Ma basalt tilted 20° to 25° overlies these units (Tb_1 of *Monsen et al.* [1992]). Younger units in the area which overlie the basalt are flat-lying. These include the 8.2 Ma gravel of Sober-up Gulch (average of three K-Ar dates, 8.2±0.4 Ma on biotite, 8.7±0.2 Ma on K-feldspar, and 7.7±0.1 Ma, hand-picked K-feldspar, analyzed from a tuff layer and reported by *Monsen et al.* [1992]), and the 7.6-Ma Spearhead Member of the Stonewall Flat Tuff [*Dieno et al.*, 1989].

Faults are important controls for mineralization in Fluorspar Canyon, which implies that mineralization postdated faulting [*Greybeck and Wallace*, 1991; *Weiss et al.*, 1991]. At the Secret Pass Zone of mineralization in Fluorspar Canyon (Figure 1), the mineralized hanging wall of the Fluorspar Canyon fault is in contact with nonmineralized Paleozoic sedimentary rocks in the footwall [*Greybeck and Wallace*, 1991]. Mineralization is hosted in the 13.2 Ma Bullfrog Tuff, and related alteration can be traced into the overlying 12.8 Ma Topopah Spring Tuff [Weiss, 1996]. Some movement along the Fluorspar Canyon fault must therefore be younger than 12.8 Ma.

An east-to-west progression of tilting is evident with respect to both inception and cessation. Tilting in the hanging wall of the breakaway began before 12.7 Ma and ceased by 11.6 Ma, but in the central and western Fluorspar Hills, tilting continued after 11.45 Ma and ceased by 8.2 Ma. The greatest tilting took place from 12.7 to 11.6 Ma, as documented by the generally steep dips (40-90°) of volcanic units older than 11.6 Ma [*Monsen et al.*, 1992]. In the central and western Fluorspar Hills, units 11.6 to 10.7 Ma dip more gently (25-45°) and units 8.2 Ma and younger are flat-lying.

Age of Movement along the Tates Wash and Bare Mountain faults

Alunite dated at 12.2±0.4 Ma (K-Ar [*McKee and Bergquist*, 1993]) is present in the hanging wall of the Tates Wash fault in conglomeratic bedded tuff that underlies the 11.62 Ma rhyolite of Fluorspar Canyon [*Weiss*, 1996]. The same conglomeratic unit elsewhere underlies the Crater Flat Tuff and is therefore older than 13.45 Ma. Nearby in the footwall are rounded monomineralic clasts of fine-grained 11.2±0.3 Ma alunite (K-Ar [*McKee and Bergquist*, 1993]) within a pipe-like body of hydrothermal breccia in silicified Paleozoic dolomite. *Weiss* [1996] interpreted the alunite clasts to be related to shallow hydrothermal activity. If the Tates Wash fault localized the mineralization [*Greybeck and Wallace*, 1991; *Weiss*, 1996; *Weiss et al.*, 1991], then it must have undergone displacement and accommodated uplift of the footwall to shallow depths prior to 12.2 Ma.

Variably altered 13.9 Ma rhyolite porphyry dikes (K-Ar on

biotite [*Monsen et al.*, 1992]) with coarse granophyric textures and hypersaline fluid inclusions intrude the footwall of the Tates Wash fault [*Weiss*, 1996]. *Weiss* [1996] interpreted the textures and fluid inclusions to indicate that the dikes were emplaced at several kilometers depth, and inferred that 1-2 km of footwall uplift along the Tates Wash fault took place between the dike emplacement at 13.9 Ma and the shallow alunitic mineralization at 12.2 Ma. There is evidence for Quaternary movement along the south side of Tates Wash. From a trench across the fault, *Monsen et al.* [1992] reported that older alluvial fan deposits (Pliocene or early Pleistocene) are faulted, but intermediate-age alluvial fan deposits (middle and late Pleistocene) are not.

Carr and Parrish [1985] reported that avalanche breccias of Paleozoic carbonate rocks, shed from the scarp of the Bare Mountain fault, were intersected between 12.7 Ma Tiva Canyon Tuff and 11.6 Ma Rainier Mesa Tuff in drill hole USW VH-2 in Crater Flat (Figure 1). Thus Paleozoic rocks at Bare Mountain had surfaced by 11.6 Ma [*Carr and Parrish*, 1985; *Faulds et al.*, 1994]. Movement younger than 11.6 Ma is implied by rock avalanches of 11.6 Ma Rainier Mesa Tuff that were shed from east facing scarps along Tram Ridge and along another ridge in north central Crater Flat (F.W. Simonds and C.J. Fridrich, written communication, 1995).

At the south end of Bare Mountain, south of Steve's Pass (Figure 1), a second avalanche of Paleozoic rocks overlies a 10.5±0.1-Ma basalt (K-Ar, whole rock [*Swadley and Carr*, 1987]) and was also intersected in drill hole USW VH2 (Figure 1) at a depth of 360 m [*Carr and Parrish*, 1985]. Because the breccia directly overlies the basalt, with no intervening material, it is probably also about 10.5 Ma in age. The lack of avalanche deposits in the upper 360 m in drill hole USW VH2, the shallowness of the basalt, and the presence of flat-lying 3.7 Ma and younger volcanic rocks at the surface within Crater Flat [*Carr*, 1988] suggest that the Bare Mountain fault has had a low average rate of displacement since 10.5 Ma. This is consistent with the analysis of *Fridrich et al.* [1997], who estimated that the current rate of extension within the Crater Flat basin is only 1% of what it was during the main extensional pulse at 12.7-11.6 Ma, when the basin opened. There is, however, documented late Quaternary and possibly Holocene movement along the Bare Mountain fault [*Klinger and Anderson*, 1994; *Reheis*, 1988].

Age of Normal Faulting in the Lower Plate at Bare Mountain

Monsen et al. [1992] reported that one east dipping normal fault in the lower plate at Bare Mountain is cut by a quartz latite dike which they considered to be part of the same family of dikes dated elsewhere at Bare Mountain at 13.9 Ma. In other exposures, they reported that similar dikes are faulted, but are offset less than the country rock. Faulting therefore began prior to and continued after 13.9 Ma, consistent with speculations (discussed previously) on the early movement history of the Bare Mountain fault. Some east dipping faults cannot be active because they are cut by the east-west striking segment of the Gold Ace fault (Figure 1). None of the east dipping faults, other than the Bare Mountain fault, show evidence of Quaternary slip.

Monsen et al. [1992] show the Gold Ace fault cutting several east dipping faults (Figure 1). The fault also cuts a 16.9±0.5 Ma basaltic dike (dated $^{40}Ar/^{39}Ar$ on hornblende from sample TH-SP-9, this study) and is itself cut by the Fluorspar Canyon fault. Because movement along the Fluorspar Canyon fault was over by 8.2 (discussed previously), movement along the Gold Ace fault must be younger than 16.9 and older than 8.2 Ma, and movement along the truncated east dipping faults must be older than 8.2 Ma.

This is consistent with the direct truncation of several east dipping faults by the Fluorspar Canyon fault.

Age of Normal Faulting in the Upper Plate in the Bullfrog Hills

No major angular discordances are present between the Lithic Ridge, Bullfrog, Tiva Canyon, Rainier Mesa, and Ammonia Tanks Tuffs in the Bullfrog Hills [*Maldonado*, 1990b; *Weiss*, 1996]. Subsequent tilting was coeval with deposition of the TLBH. From bottom to top, the TLBH consists of a basalt (Tb2 of *Maldonado and Hausback* [1990], and Tb4 of *Ransome et al.* [1910]), followed by the rhyolite lavas and tuffs of Rainbow Mountain, followed by latite and andesite flows [*Maldonado and Hausback*, 1990]. Seven stratigraphically inconsistent K-Ar dates ranging from 9.6±0.3 to 11.1±0.4 Ma have been reported from the TLBH [*Marvin and others*, 1989; *Marvin and Cole*, 1978; *Morton et al.*, 1977; *Noble et al.*, 1991] and were summarized by *Weiss* [1996]. Based on these seven dates, it was concluded that the TLBH are 10.5 to 10.0 Ma in age [*Conners et al.*, 1995; *Weiss*, 1996; *Weiss et al.*, 1991]. A revised interpretation is indicated by the correlation of the 10.7 Ma basalt from the Fluorspar Hills with the basalt at the bottom of the TLBH (C.J. Fridrich, oral communication, 1995) and by two new dates: 10.56 Ma was obtained from a rhyolite ash flow tuff near the bottom of the Rainbow Mountain sequence and 10.33 Ma was obtained from a latite which overlies the sequence, both $^{40}Ar/^{39}Ar$ laser fusions on sanidine [*Eng et al.*, 1996]. Based on these data, the TLBH is 10.7-10.33 Ma.

An angular discordance of about 15-20° occurs between the 10.7 Ma basalt and the 10.56 Ma base of the Rainbow Mountain sequence about 1 km east of the Barrick Gold Bullfrog Mine (Figure 1) (D.R. Boden, written communication, 1996). Dips become progressively shallower within the Rainbow Mountain sequence and overlying latites, from about 45-50° at the 10.56 Ma base to about 15° at the 10.33 Ma latite (D.R. Boden, written communication, 1996; similar observations were made by *Weiss et al.* [1990]). Tilting was therefore active from 10.7 to 10.3 Ma and continued after 10.3 Ma. The 7.6 Ma Spearhead Member of the Stonewall Flat Tuff overlies parts of the TLBH and, according to paleomagnetic data, is not tilted [*Maldonado*, 1990b]. An 8.1±0.4 Ma basalt (K-Ar, whole rock [*Marvin et al.*, 1989]) conformably underlies the Spearhead Member in the Bullfrog Hills. Layers of coarse breccia, locally containing enormous blocks of Rainier Mesa Tuff, Ammonia Tanks Tuff, and other tuffs, interfinger with units of the TLBH and have been interpreted to be landslide megabreccias and debris flow deposits shed from scarps or steep topography [*Weiss et al.*, 1990; *Minor and Fleck*, 1994]. Thus, faulting and tilting was active from 10.7 to 10.3 Ma, continued after 10.3 Ma, and was over by 8.1 Ma.

The main body of vein material at the Original Bullfrog Mine follows a normal fault [*Maldonado*, 1990b; *Weiss*, 1996]. Two splits of adularia from altered 14.0 Ma Lithic Ridge Tuff yielded a conventional K-Ar date of 8.7±0.3 Ma and a $^{40}Ar/^{39}Ar$ multigrain fusion date of 9.2±0.3 Ma [*McKee and Bergquist*, 1993]. The distinct contrast in wallrock alteration exposed in the footwall and hanging wall of the mined fault vein suggests that about 0.5 km of movement postdated mineralization (D.R. Boden, written communication, 1996; similar observations were made by *Weiss* [1996] and *Weiss et al.* [1991]). Drilling shows that the fault soles into the detachment (D.R. Boden, written communication, 1996) and thus the detachment was active at about ~9 Ma.

Table 2. Summary of Thermochronologic Data From the Lower Plate in the Bullfrog Hills and the Northwest Part of Bare Mountain

Sample	Rock Type	Mineral	Method	Age ± 2σ, Ma	Source	Notes
			Bullfrog Hills			
BF-MO-5c	granite	muscovite	Ar-Ar step heating	14.24±0.12	Figure 2	2,6
		K-feldspar	Ar-Ar step heating	see text	Figure 2	2
BF-TH-9ab	amphibolite	hornblende	Ar-Ar step heating	77.7±1.6	Figure 2	2,5
		apatite	fission track	10.0±1.5	Table 4	2
		zircon	fission track	9.2±1.0	Table 4	2
		zircon	U-Pb	1743±5	Table 3	3
		sphene	fission track	8.9±1.4	Table 4	2
		sphene	U-Pb	70±1	Table 3	2
		apatite	U-Pb	28±1	Table 3	2
BF-TH-10	schist	apatite	fission track	10.6±2.0	Table 4	2
		zircon	fission track	11.2±2.8	Table 4	2
DF-1796	gneiss	muscovite	K-Ar	11.2±1.1	*McKee* [1983]	2
TSV-296-80	gneiss	muscovite	K-Ar	16.3±0.4	*Marvin et al.* [1989]	2
C82BM-455	schist	biotite	K-Ar	10.5±0.3	Table 5	2
C82BH-469	pegmatite	muscovite	K-Ar	13.6±0.3	Table 5	2
JN85B-2	schist	muscovite-1	K-Ar	14.1±0.4	Table 5	2
		muscovite-2	K-Ar	14.2±0.4	Table 5	2
73082-8	amphibolite	hornblende	K-Ar	65.1±1.6	Table 5	2
			Northwest Bare Mountain			
BM-TH-14ab	schist	muscovite	Ar-Ar laser fusions	55.7±0.6	Table A3	2,4
		biotite	Ar-Ar step heating	46.2±0.6	Figure 2	2,5
		apatite	fission track	11.1±1.9	Table 4	2
		apatite	U-Pb	60 ± 5	Table 3	2,7
		zircon	fission track	12.6±1.6	Table 4	2
BM-DC-25	granite	muscovite	Ar-Ar laser fusions	53.4±0.6	Table A3	2,4
		K-feldspar	Ar-Ar step heating	see text	Figure 2	2
BF-12a	schist	biotite	K-Ar	54.0±1.3	Table 5	2
		muscovite	K-Ar	57.4±1.4	Table 5	2
TH-SP-21	granite	K-feldspar	Ar-Ar step heating	see text	Figure 2	2
TH-SP-9	basaltic dike	hornblende	Ar-Ar step heating	16.9±0.5	Figure 2	1,6
BF-17	schist	biotite	K-Ar	38.5±1.0	Table 5	2
JN85B-3	schist	muscovite-1	K-Ar	45.2±0.3	*Monsen et al.* [1992]	2
		muscovite-2	K-Ar	44.3±0.3	*Monsen et al.* [1992]	2
		biotite-1	K-Ar	48.6±0.3	*Monsen et al.* [1992]	2
		biotite-2	K-Ar	49.2± 0.4	*Monsen et al.* [1992]	2
83-89	schist	muscovite	K-Ar	51.6±1.3	*Monsen et al.* [1992]	2
		biotite	K-Ar	46.0±1.2	*Monsen et al.* [1992]	2

Notes 1, Basaltic dike is cut by the Gold Ace fault, date is age of the dike; 2, cooling age; 3, absolute age of basement metamorphism; 4, oldest age obtained in a series of total laser fusions of two or three crystals; 5, plateau age; 6, isochron age; 7, minimum age.

Thermochronology of Lower Plate Rocks

For the $^{40}Ar/^{39}Ar$ and K-Ar methods, argon closure temperatures are taken from *McDougall and Harrison* [1988]: 500°C for hornblende, 300°C for biotite, and 350°C for muscovite. The $^{40}Ar/^{39}Ar$ analytical method follows *McIntosh and Cathers* [1994]. Argon closure in K-feldspar is treated differently following the multiple diffusion domain (MMD) method developed by *Lovera et al.* [1989]. Annealing temperatures for fission track analyses are approximately 285°C for sphene [*Harrison et al.*, 1979], 205°C for zircon [*Zeitler et al.*, 1982], and 120°C for apatite [*Dokka et al.*, 1986]. A closure temperature of 750°C or higher is commonly assumed for the U-Pb dating of zircon. For the U-Pb dating of apatite, *Cherniak et al.* [1991] determined that grains of the same size as those we analyzed (-100 to +150 mesh) undergo closure at ~475°C for a cooling rate of 10°C m.y.$^{-1}$. For the U-Pb dating of sphene, a field-calibrated closure temperature of 500°C was determined by *Gascoyne* [1986]. More recently, however, Cherniak [1993] determined a higher closure temperature of 560°C for grains of similar size as those we analyzed and a cooling rate of 10°C m.y.$^{-1}$, and this value is adopted for our

study. Because of the high ratio of common to radiogenic Pb in the sphene and apatite, the ages of these minerals were calculated by assuming isotopic equilibrium with coexisting plagioclase at the time of closure. For apatite, sufficient enrichment in radiogenic Pb to produce reliable ages was attained only for the $^{206}Pb/^{238}U$ method. A summary of the thermochronologic data, which includes both previously published and new data, is provided in Table 2. The details of new data are given in Tables A1-A3[1] ($^{40}Ar/^{39}Ar$) and Table 3 (U-Pb), Table 4 (fission track), and Table 5 (conventional K-Ar).

Northwest Part of Bare Mountain

Thermochronology samples were collected west of the Gold Ace fault, three from schist of the Wood Canyon Formation

Table 3. U-Th-Pb Isotopic Data for Zircon, Sphene, and Apatite Ages

Mineral	Concentration, ppm			Isotopic Composition of Pb, at. %				Age ±2σ, Ma			
	U	Th	Pb	^{204}Pb	^{206}Pb	^{207}Pb	^{208}Pb	$^{206}Pb/^{238}U$	$^{207}Pb/^{235}U$	$^{207}Pb/^{206}Pb$	$^{208}Pb/^{232}Th$
Sample BF-TH-9ab (Bullfrog Hills)											
Zircon (-100+200 mesh)											
Equant	495.7	97.8	132.0	0.0320	84.27	9.406	6.295	1485±14	1594±15	1739±2	1526±18
Elongate	543.3	196.9	139.8	0.0231	83.41	9.188	7.379	1430±13	1559±18	1738±2	1033±14
Sphene (-50+100 mesh)											
Light yellow	214.1	100.4	6.52	0.8747	44.96	14.96	39.21	67±1	65±2	--	73±2
Dark yellow	271.9	209.4	7.83	0.7892	46.37	13.77	39.07	70±1	68±1	--	69±1
Apatite (-100+150 mesh)	18.08	4.72	6.31	1.345	24.66	20.94	53.05	28±1	--	--	--
Plagioclase	0.070	0.017	7.83	[$^{206}Pb/^{204}Pb$ = 17.546; $^{207}Pb/^{204}Pb$ = 15.548; $^{208}Pb/^{204}Pb$ = 39.168]							
Sample BM-TH-14ab (Bare Mountain)											
Apatite (-100+150 mesh)	10.06	2.12	6.07	1.297	26.04	20.56	52.11	60±5	--		
Plagioclase	0.288	0.502	6.17	[$^{206}Pb/^{204}Pb$ = 19.077; $^{207}Pb/^{204}Pb$ = 15.806; $^{208}Pb/^{204}Pb$ = 40.210]							

Decay constants are ^{238}U = 1.55125x10^{-10} yr^{-1}; ^{235}U = 9.8485x10^{-10} yr^{-1}; ^{232}Th = 4.9375x10^{-11} yr^{-1}; $^{238}U/^{235}U$ = 137.88. Isotopic composition of common lead was assumed in the calculation of the zircon data to be ^{204}Pb:^{206}Pb:^{207}Pb:^{208}Pb = 1:15.76:15.32:35.40. Isotopic composition of common lead for the sphene and apatite age calculations was taken to be that of the coexisting plagioclase corrected for in situ radioactive decay, 70 Ma for sphene and 28 Ma for apatite in sample BF-TH-9ab, and 60 Ma for apatite in sample BM-TH-14ab

Table 4. Fission Track Data for Lower Plate Samples From the Northwest Part of Bare Mountain and the Bullfrog Hills

Sample	Mineral	Fossil Track Density, tracks cm^{-2}	Fossil Track Count, tracks	Induced Track Density, tracks cm^{-2}	Induced Track Count, tracks	Number of Grains	Standard Track Density, tracks cm^{-2}	Standard Track Count, tracks	Zeta	Date ±2σ, Ma
		Northwest Bare Mountain								
BM-TH-14ab	apatite	1.885x10^5	151	3.147x10^6	2521	20	3.353x10^4	2406	11049.0	11.1±1.9
	zircon all*†	5.533x10^6	943	7.803x10^6	1330	10	2.565x10^5	2644	337.5	30.6±5.3
	zircon large§	2.296x10^6	386	7.886x10^6	1326	10	2.565x10^5	2644	337.5	12.6±1.6
		Bullfrog Hills								
BF-TH-9ab	apatite	2.786x10^5	189	5.245x10^6	3558	10	3.395x10^4	2406	11049.0	10.0±1.5
	zircon	3.046x10^6	430	1.432x10^7	2022	9	2.573x10^5	2644	337.5	9.2±1.0
	sphene*	9.754x10^5	407	4.534x10^6	1892	10	2.590x10^5	2644	319.3	8.9±1.4
BF-TH-10	apatite	1.499x10^5	113	2.681x10^6	2021	11	3.438x10^4	2406	11049.0	10.6±2.0
	zircon*	3.628x10^6	544	1.410x10^7	2115	6	2.582x10^5	2644	337.5	11.2±2.8

Age determinations and calculations by R.A. Zimmermann (U.S. Geological Survey, Denver, 1995).
*Sample failed χ^2 test for homogeneity. Dates were calculated by performing a weighted average and weighted standard deviation (σ) of counts among individual grains.
†Fossil tracks counted include both large-diameter and small-diameter pits.
§Fossil tracks counted include only large-diameter pits.

Table 5. Conventional K-Ar Data for Lower Plate Samples From the Northwest Part of Bare Mountain and the Bullfrog Hills

Sample	Rock Type	Latitude N	Longitude W	Age±2σ, Ma	Mineral	K_2O, wt %	$^{40}Ar_{rad}/^{40}Ar_{tot}$	$^{40}Ar_{rad}$, mol/g	Collected by
Northwest Bare Mountain									
BF-12ab*	Schist	36°52'59"	116°43'48"	57.4±1.4	Muscovite	9.23	0.79	7.75×10^{-10}	T.D. Hoisch
				54.0±1.4	Biotite	8.85	0.70	6.95×10^{-10}	
BF-17*	Schist	36°53'29"	116°45'08"	38.5±1.0	Biotite	9.15	0.78	5.13×10^{-10}	T.D. Hoisch
Bullfrog Hills									
JN85B-2*	Schist	36°54'	116°54'	14.1±0.4	Muscovite-1	10.39	0.74	2.11×10^{-10}	J.K. Nakata
				14.2±0.4	Muscovite-2	10.39	0.66	2.14×10^{-10}	
C82BH-469†	Pegmatite	36°54'02"	116°53'35"	13.6±0.3	Muscovite	10.945	0.35	2.158×10^{-10}	M.D. Carr
73082-8†	Amphibolite	36°53'57"	116°53'44"	65.1±1.6	Hornblende	0.8555	0.44	8.164×10^{-11}	S.A. Monsen
C82BM-455†	Schist	36°53'36"	116°52'45"	10.5±0.3	Biotite	8.375	0.24	1.275×10^{-10}	M.D. Carr

*Argon measurements and age calculated by J.K. Nakata (U.S. Geological Survey, Menlo Park, California).
†Argon measurements and age calculated by J. Saburomaru and J.C. Von Essen (U.S. Geological Survey, Menlo Park, California).

(BM-TH-14ab, BF-12ab, and BF-17), one from a Late Cretaceous muscovite granite dike (BM-DC-25), and one from an older Cretaceous granite body (TH-SP-21) mapped by *Monsen et al.* [1992] as a fault-bounded slice directly beneath the Fluorspar Canyon fault (Figure 1). A sample from a basaltic dike (TH-SP-9) was also dated. The basaltic dike is 1 m thick, intrudes into fine-grained schist of the Carrara Formation (Cambrian), and is cut by the Gold Ace fault. Thus the age of the dike limits the age of fault movement.

The $^{40}Ar/^{39}Ar$ muscovite incremental-release spectrum from schist sample BM-TH-14ab (Figure 2) is somewhat complex but shows an overall age gradient from ~30 to 60 Ma and yields a total gas age of 53.6 Ma. The final 90% of gas evolved reveals the flattest portion of the age spectrum but yields no statistical plateau or isochron correlation. Ten individual laser fusions of two or three (100 mesh) grains each (Table A3) yielded ages between 51.3±1.8 Ma and 55.7±0.5 Ma indicating that the sample is homogeneous on an individual crystal scale and that the complexity of the age spectrum is caused by a non-uniform distribution of $^{40}Ar*$ within the micas and not related to age-discordant mica populations [*West and Lux*, 1993]. The age gradient in the first 10 % of ^{39}Ar released is thus interpreted to be related to partial Ar loss. The terminal age of ~60 Ma is a minimum estimate of when the sample passed through the closure temperature (350-400°C) of the core of the crystal. The biotite spectrum from the same sample is similar to the muscovite in form but significantly younger. The total gas age is 43.1 Ma and the flat portion yields a mean age of 46.2 Ma. The plateau age of ~46 Ma probably represents the time of cooling below ~300°C and the age gradient results from diffusive argon loss.

Zircon and apatite from BM-TH-14ab were analyzed by the fission track method (Table 4). A distribution of pit diameters was observed in the zircon grains. A date of 30.6±5.3 Ma was determined when both small and large pits were counted. This compares to 12.6±1.6 Ma when only the large pits were considered. The implication is that the sample had a long residence time at temperatures just above the annealing temperature, causing a partial annealing (shrinking) of the older (>12.6 Ma) pits. Apatite yielded a date of 11.1±1.9 Ma. A U-Pb apatite age of 60±5 Ma was obtained from BM-TH-14ab using coexisting plagioclase to correct for the common Pb isotopic composition (Table 3).

BF-12ab and BF-17 schist samples yielded conventional K-Ar biotite dates of 54.0±1.4 Ma and 38.5±1.0 Ma, respectively (Table 5). Muscovite from schist sample BF-12ab yielded 57.4±1.4 Ma (Table 5). Six additional K-Ar dates on micas from two samples of Wood Canyon Formation schist range from 44.3±0.3 to 51.6±1.3 Ma [*Monsen et al.*, 1992].

Muscovite and K-feldspar from Late Cretaceous granite sample BM-DC-25 were analyzed by the $^{40}Ar/^{39}Ar$ step-heating method (Figure 2). The muscovite results are similar to sample BM-TH-14ab and are interpreted in the same manner. The 10 laser fusion ages (two or three grains each) scatter over about 10 m.y. (Table A3) and are interpreted to reflect crystal-to-crystal variation in argon retentivity. The oldest age of ~53 Ma is taken as the best estimate for cooling below ~350°C. The K-feldspar age spectrum is discussed below.

Sample TH-SP-21 was collected from a granite for $^{40}Ar/^{39}Ar$ analysis of K-feldspar (discussed below). From the same granite, *Monsen et al.* [1992] reported a U-Pb date based on three size fractions of zircon. A U/Pb concordia plot yielded a lower and upper intercept of 98±27 Ma and 1734±212 Ma, respectively.

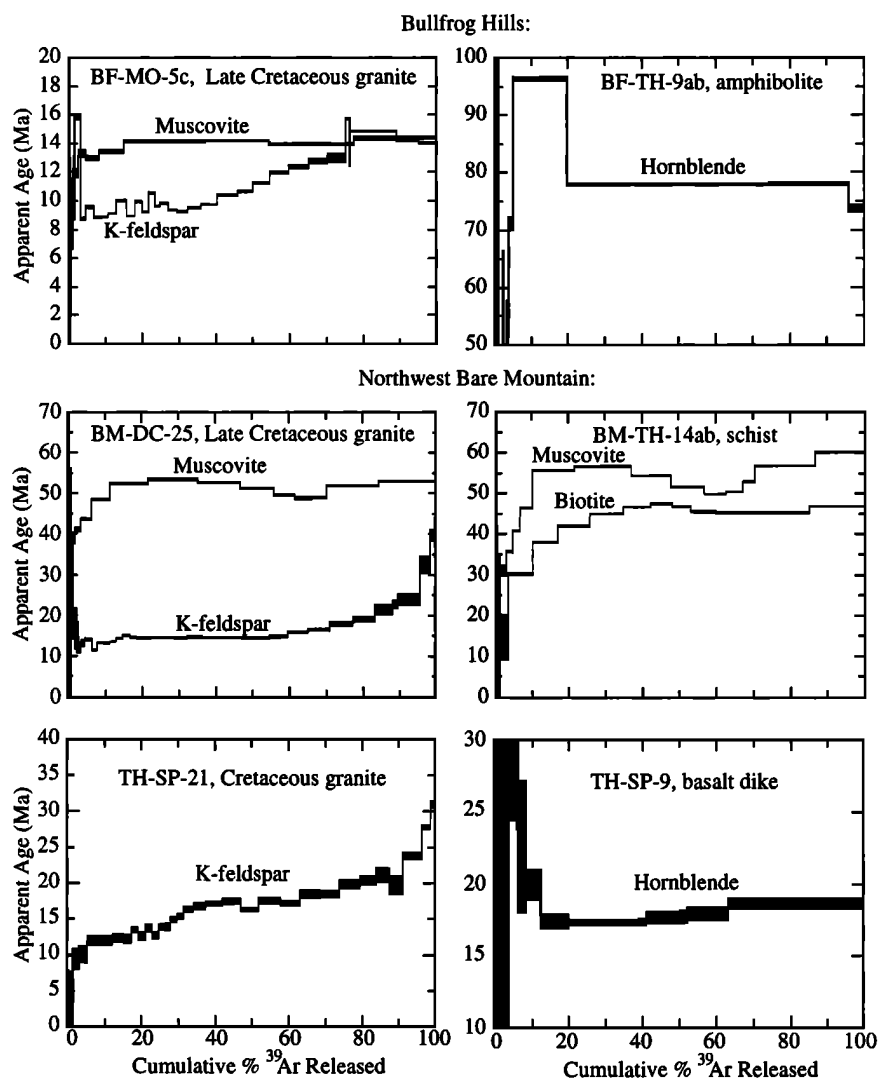**Figure 2.** $^{40}Ar/^{39}Ar$ age spectra based on data in Tables A1 and A2.

Carr [1984] reported a zircon fission track date of 25.4±1.3 Ma, which is much older than the zircon fission track date of 12.6±1.6 Ma that we obtained from sample BM-TH-14ab nearby. The difference in age could be due to differences in track retentivity during slow cooling, or the granite body may have had a different low-temperature thermal history than the schist, from which it is separated by a fault [*Monsen et al.*, 1992].

The hornblende $^{40}Ar/^{39}Ar$ age spectrum from basaltic dike sample TH-SP-9 (Figure 2) indicates relatively old ages for the first 15% of gas released and then steadily climbs from a minimum of about 17.3 Ma. Heating steps 3-9 comprise about 95% of the total gas and yield an isochron age of 16.9±0.5 Ma with a mean squared weighted deviation (MSWD) of 0.5, and a trapped $^{40}Ar/^{36}Ar_i$ value of 303.2±2.0. The isochron age is interpreted to be the age of crystallization.

Bullfrog Hills

Samples of amphibolite (BF-TH-9ab), mica schist (BF-TH-10), and a Late Cretaceous muscovite granite dike (BF-MO-5c) were collected from the lower plate of the detachment fault in the Bullfrog Hills (Figure 1). Hornblende from amphibolite sample BF-TH-9ab was dated by the $^{40}Ar/^{39}Ar$ step-heating method.

The final three heating steps comprise about 80% of the total argon and yield a mean age of 77.7±1.6 Ma. The poor resolution of the age spectrum makes for an ambiguous interpretation, but the sample likely cooled below 500°C between 70 and 80 Ma. Apatite, zircon, and sphene fission track dates from BF-TH-9ab are 10.0±1.5 Ma, 9.2±1.0 Ma, and 8.9±1.4 Ma, respectively (Table 4). These compare favorably to apatite and zircon fission track dates obtained from schist BF-TH-10: 10.6±2.0 Ma and 11.2±2.8 Ma, respectively (Table 4).

U-Pb zircon ages from BF-TH-9ab document that the lower plate rocks in the Bullfrog Hills belong to the crystalline basement that underlies the Late Precambrian and Paleozoic sedimentary sequence. Two zircon shape fractions, equant (aspect ratios of 1:1 to 1.5:1) and elongate (aspect ratios of 3:1 to 5:1) yielded ages that are about 16% and 22% discordant (respectively) and project to an upper concordia intercept of 1742.9±4.9 Ma and a lower intercept of 34±40 Ma (Figure 3). The zircons were euhedral and prismatic with simple to complex bipyramidal terminations, clear to slightly turbid due to cracks and minor inclusions, and colorless to slightly yellow or smoky and had mirrorlike to very slightly etched faces and sharp to very slightly rounded edges. All zircons appeared to belong to a single population with
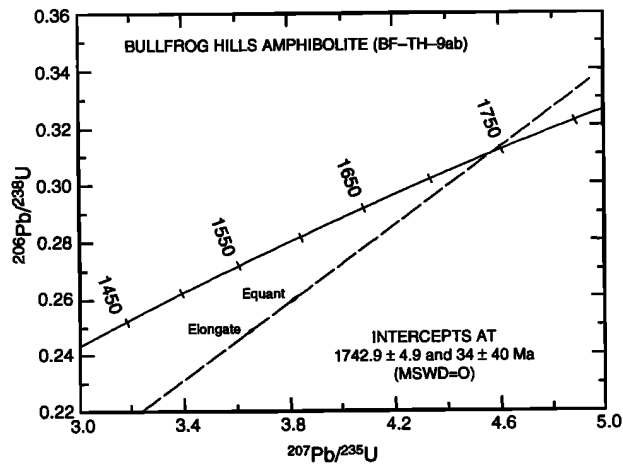
Figure 3. Concordia plot of U-Pb zircon data for amphibolite sample BF-TH-9ab.

Because the argon kinetics for each K-feldspar are determined by the release of ^{39}Ar in the laboratory, extracting meaningful thermal histories from K-feldspar age spectra relies on the assumption that the release of argon in the laboratory occurs by the same mechanism and is controlled by the same boundaries as in nature. Clearly, high degrees of alteration and porosity [*Parsons et al.*, 1988; *Burgess and Parsons*, 1994], formation of K-bearing fluid inclusions [*Burgess et al.*, 1992; *Turner and Wang*, 1992; *Harrison et al.*, 1993], laboratory induced problems [*Foland*, 1994] or substantial modification of the domains at low-temperature would manifest themselves by yielding geologically irrelevant and/or internally inconsistent thermal histories. Several studies demonstrate a good correlation between the argon kinetics derived using the MDD method and age spectra for most plutonic K-feldspars that have not undergone low-temperature alteration [e.g., *Lovera et al.*, 1989, 1991, 1993; *Harrison et al.*, 1992; *Leloup et al.*, 1993; *FitzGerald and Harrison*, 1993; *Lee*, 1994]. For this to be true, the crystallographic features which presumably impart the domainal behavior in K-feldspar must be formed and remain stable above the argon closure temperature of
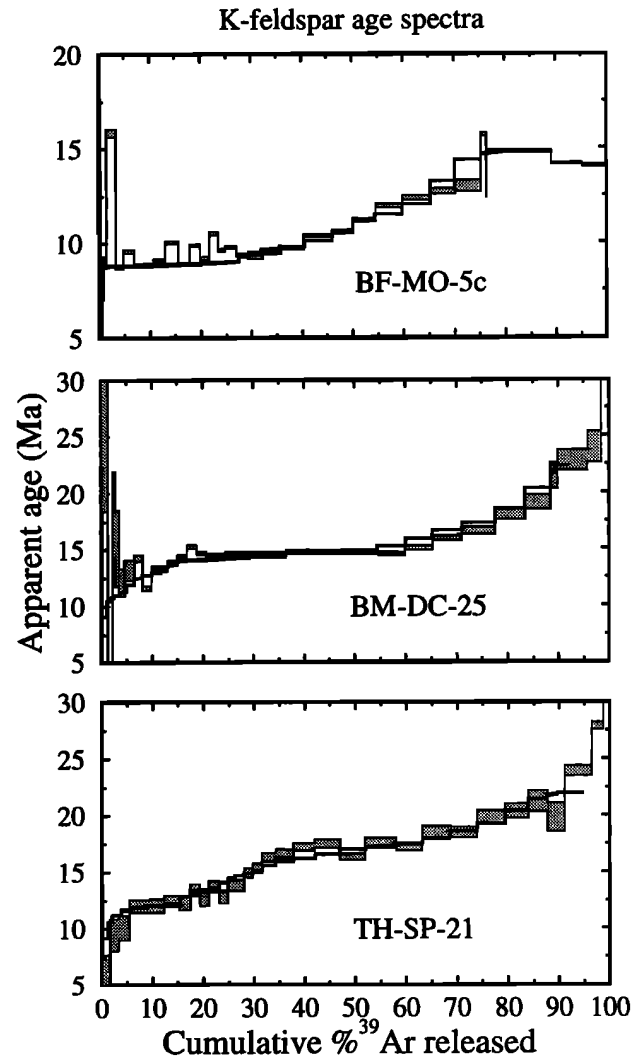
no visible evidence of cores or multiple growth zones. The good crystallinity and homogeneity suggest that the zircons crystallized in the present host rock rather than being of xenocrystic or detrital origin. Because primary igneous zircons, especially of a coarser size, are rare in basalts, these zircons are interpreted to be of metamorphic origin. The 1742.9±4.9 Ma date is interpreted as the age of the metamorphism with only minor disturbance of the isotopic system superimposed in Late Cretaceous or Tertiary time. U-Pb apatite and U-Pb sphene ages of 28±2 Ma and 70±2 Ma, respectively, were also obtained from BF-TH-9ab (Table 3).

Muscovite and K-feldspar from granite sample BF-MO-5c were dated by the ^{40}Ar/^{39}Ar step-heating method. The muscovite age spectrum (Figure 2) is essentially flat for more than 80% of the gas released and yields a corresponding isochron age of 14.24±0.12 Ma. The relatively high MSWD of 12 for the isochron may be related to the apparent slight age gradient observed in the age spectrum. The age of 14.2 Ma is taken as the time this sample cooled through the muscovite closure temperature of 350°C. The K-feldspar age spectrum is discussed later on.

There are two previously published conventional K-Ar dates on muscovite from schists collected from the lower plate of the Bullfrog detachment, 11.2±1.1 Ma [*McKee*, 1983] and 16.3±0.4 Ma [*Marvin et al.*, 1989]. Five additional dates are reported in Table 5, two muscovite dates on a schist (14.1±0.4 Ma, 14.2±.04 Ma), a biotite date on a second schist (10.5±0.3 Ma), a muscovite date from a Late Cretaceous pegmatite intruded into the metamorphic rocks (13.6±0.3 Ma), and a hornblende date from an amphibolite (65.1±1.6 Ma).

K-feldspar Thermochronology

Lovera et al. [1989] showed that complex features in K-feldspar ^{40}Ar/^{39}Ar age spectra could be explained through the use of a multiple diffusion domain model (MDD). This model views K-feldspars as containing a discrete distribution of diffusion domain sizes which implies multiple argon closure temperatures within a single sample. The implication of this is that a continuous record of the thermal history, typically between about 150 and 350°C, may be recorded within the diffusion domains. Small diffusion domains provide information about the low-temperature history, and the higher-temperature history is given by the large diffusion domains.

Figure 4. Comparisons between K-feldspar ^{40}Ar/^{39}Ar age spectra and MDD models. The solid lines are model age spectra calculated from the kinetic parameters in Figure 5 and thermal histories in Figures 6 and 7.
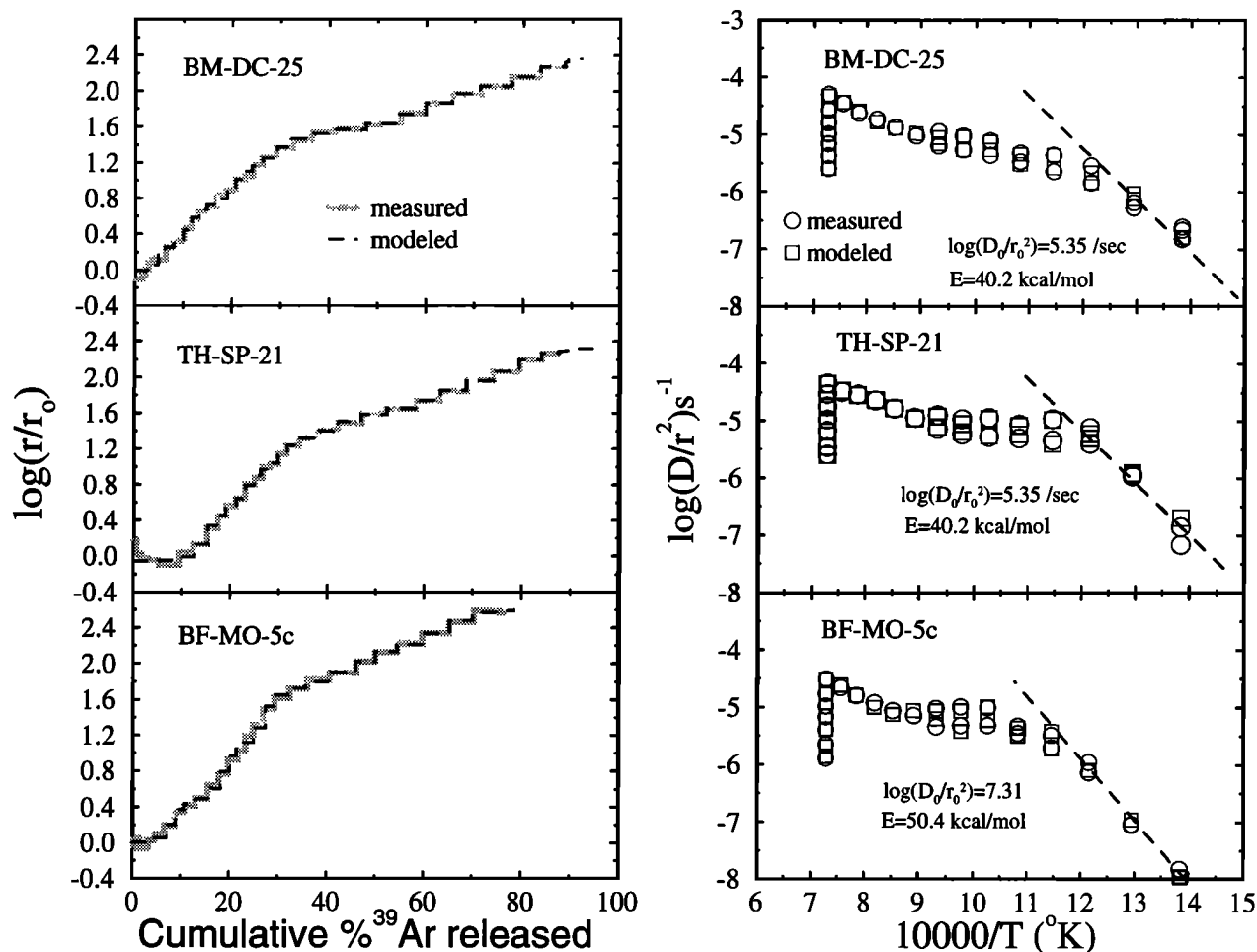
Figure 5. Arrhenius and $\log(r/r_o)$ plots for K-feldspar $^{40}Ar/^{39}Ar$ data. The dashed line on the Arrhenius plots is the reference Arrhenius law used to construct the $\log(r/r_o)$ plots. The measured diffusion coefficients were closely simulated by the parameters given in Table 6. The data for the argon extracted at or above 1100°C due were not included in the models due to the melting of the samples in the laboratory.

the domain. The strongest argument in support of the MDD method is that nearly identical and geologically reasonable thermal histories have been obtained from adjacent samples which display highly contrasting argon kinetic parameters [*Heizler et al.*, 1988; *Heizler and Harrison*, 1992; *Leloup et al.*, 1993; *Lovera et al.*, 1989].

The $^{40}Ar/^{39}Ar$ age spectra for K-feldspar are shown in figure 2 and compared to models generated using the MDD method in figure 4. The K-feldspar age spectra were closely simulated by the MDD models and thus the age gradients are not believed to result from excess argon contamination. The MDD models require argon diffusion coefficients which were determined from the ^{39}Ar released and the laboratory heating schedule using Arrhenius plots and assuming a plane slab geometry (Figure 5). The activation energy (E) for each sample was obtained from the slope of the initial diffusion coefficients and is constrained to only about ±10% due to significant scatter in the data presumably related to the low volume fraction of the smallest diffusion domain. The overall pattern of diffusion coefficients (Figure 5) is a reflection of the variation in length (r) and volume faction (ρ) of the diffusion domains. The kinetic parameters ($\log D/r^2$ and ρ, Table 6) for each sample were obtained by applying the apparent E and modeling the Arrhenius plot as a distribution of diffusion

domains [*Lovera et al.*, 1989]. The K-feldspar samples in this study were analyzed too long after irradiation to detect ^{37}Ar, which is not a problem because it has a negligible effect on the calculated age spectra.

The $\log(r/r_o)$ plots shown in figure 5 link the diffusion coefficient to the amount of ^{39}Ar contained within by each datum on the Arrhenius plot. The advantage to this diagram over the Arrhenius plot is the relative ease of visualization of the domain distribution. The $\log(r/r_o)$ diagram is derived from comparing the measured diffusion coefficients to a reference Arrhenius law. The reference Arrhenius law for each sample is defined by the initial linear segment on the Arrhenius plot and shown by the dashed lines in figure 5. The value r_o is the diffusion length associated with the reference Arrhenius law and r represents the length scale necessary to account for the deviation from the reference line. The $\log(r/r_o)$ diagram ends before 100% ^{39}Ar release because the sample begins to melt at extraction temperatures above 1100°C and thus no volume diffusion information is obtainable for this portion of the data (Figure 5). Finally, using the kinetic parameters, the thermal history is retrieved by repeated forward modeling of the age spectrum.

The absolute temperature of the modeled thermal history is highly controlled by the choice of activation energy, but the form

Table 6. Kinetic Parameters for K-feldspar Diffusion Models

	BF-MO-5c	BM-DC-25	TH-SP-21
E, kcal/mol	50.4	40.2	40.2
$\log(D/r_1)$	9.456	7.918	7.096
ρ_1	0.0609	0.0312	0.1258
$\log(D/r_2)$	7.897	6.746	5.858
ρ_2	0.1075	0.0587	0.0773
$\log(D/r_3)$	6.547	5.411	4.800
ρ_3	0.0820	0.0788	0.0569
$\log(D/r_4)$	4.577	4.372	3.663
ρ_4	0.1402	0.0700	0.0755
$\log(D/r_5)$	3.571	2.779	2.698
ρ_5	0.1821	0.2576	0.2003
$\log(D/r_6)$	2.107	1.862	1.927
ρ_6	0.4272	0.1759	0.1839
$\log(D/r_7)$		1.332	0.980
ρ_7		0.1311	0.1438
$\log(D/r_8)$		0.550	0.550
ρ_8		0.1967	0.1365

ρ is the volume fraction of each domain.

of the thermal history is governed by the overall diffusion length-scale distribution and the age spectrum. The E of 50.4 kcal/mol for sample BF-MO-5c is provided by the slope of the first seven diffusion coefficients. Samples BM-DC-25 and TH-SP-21 have nearly identical diffusion coefficients and thus the initial linear array for both samples were combined to yield an apparent E of 40.2 kcal/mol that is used for both samples (Figure 5).

The model age spectrum for BM-DC-25 (Figure 4) was obtained from the thermal history shown in Figure 5. The flat portion of the age spectrum at 14.3 Ma requires rapid cooling ($\sim$100°C m.y.$^{-1}$). The age gradients from 10 to 12 Ma and from 14 Ma to 25 Ma were simulated by slower cooling rates of 10-20°C m.y.$^{-1}$ and $\sim$5°C m.y.$^{-1}$, respectively, for these time intervals (Figure 6).

The granite body from which sample TH-SP-21 was taken is leucocratic, intensely fractured, iron stained along fractures, propylitically altered, and friable. Although TH-SP-21 K-feldspar is altered, it provided both a sensible age spectrum and Arrhenius relationship (Figures 4 and 5). The thermal history shown in figure 6 yielded a model age spectrum that is in good agreement with the measured spectrum (Figure 4) and indicates relatively rapid cooling ($\sim$22°C m.y.$^{-1}$) from about 17 to 12 Ma. Prior to 17 Ma, the cooling rate appears to have been significantly slower (Figure 6), thus producing the age gradient for the final 40% of ^{39}Ar released (Figure 4).

The age gradients for the last 40% of gas released from both BM-DC-25 and TH-SP-21 are interpreted as representing the concentration distribution for ^{40}Ar* and are not caused by excess argon. The kinetic parameters for these samples simulate the age gradients when cooling from 330°C at a rate of about 2-5°C m.y.$^{-1}$ is used between 25 Ma and 30 Ma. This cooling rate is well constrained from about 22 to 17 Ma for TH-SP-21 and 25-14 Ma for BM-DC-25, but the final 10% of the age spectrum cannot be unambiguously modeled as there is no control on the kinetic parameters. The apparent ages older than 25 Ma are, however, consistent with slow cooling prior to 25 Ma and are interpreted as such. The noise in the initial portion of the age spectra for these samples also allows a range of thermal histories for the period between 10 Ma and 14 Ma (Figure 6).
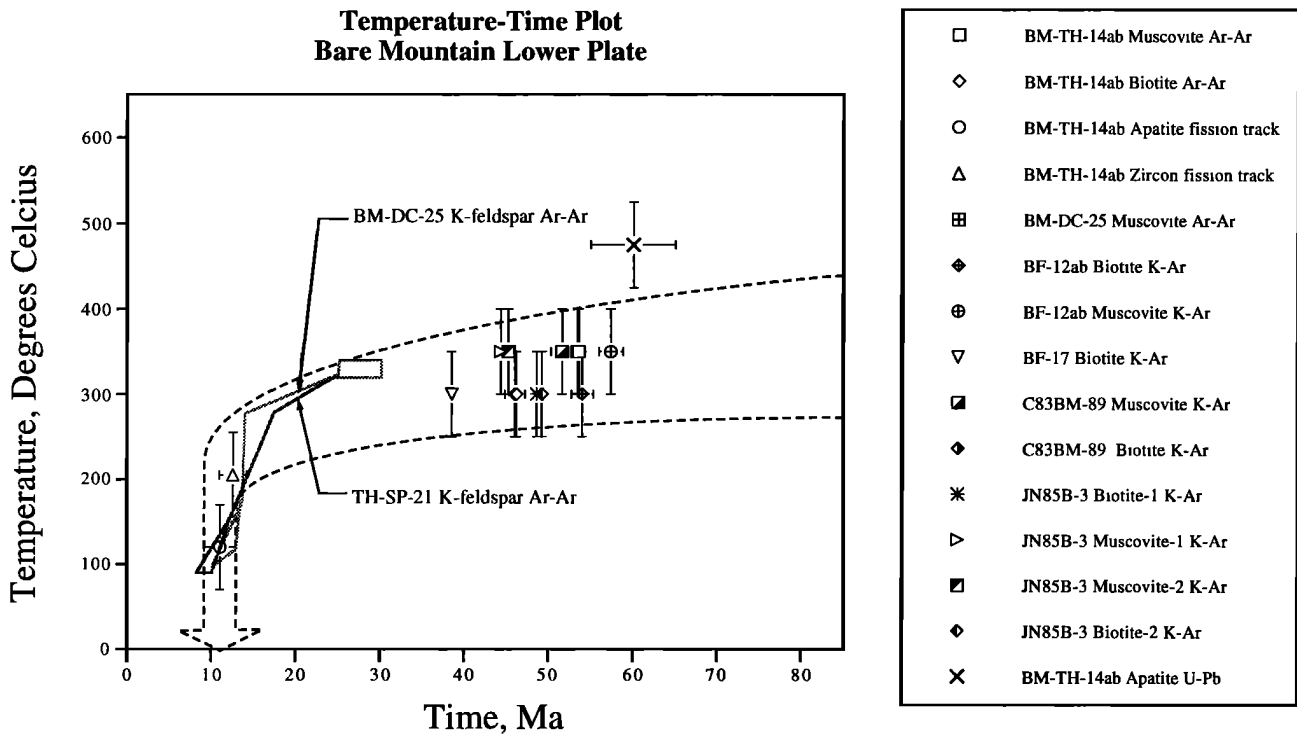

Figure 6. Temperature-time plot for lower plate rocks from northwestern Bare Mountain, based on data reported in Table 2. Dashed arrow shows inferred temperature-time path. The K-feldspar thermal histories (TH-SP-21 and BM-DC-25) are derived from modeling the age spectra (Figure 2) using the measured diffusion parameters shown in Figure 5. The windows on either end of the temperature histories represent uncertainty in the age spectrum and domain distribution.

The K-feldspar age spectrum from sample BF-MO-5c shows an age gradient from ~9 to 14 m.y. (Figure 2). The alternating old and young steps over the first 30% of gas release is commonly observed for K-feldspars step-heated with isothermal duplicate steps [e.g., *Harrison et al.*, 1994] and is inferred to be related to the preferential release of excess argon hosted in fluid inclusions during the first heating step at a given temperature [*Harrison et al.*, 1993; 1994]. Using the relationship of Cl to excess Ar described by *Harrison et al.* [1994] to correct the measured apparent ages, the first 30% of the age spectrum is inferred to have an age of 8.8±0.4 Ma with no significant gradient. The log(r/r_o) plot (Figure 5) indicates a nearly 100°C increase in closure temperature across the first 30% of the age spectrum and thus the model thermal history (Figure 7) incorporates cooling from 325°C to 150°C from 9-9.5 Ma to 8.5-9 Ma. Cooling to 150°C by 8.5 Ma is necessary to preserve the flatness of the measured age spectrum for this time interval. The age gradient from 9 to 14 Ma requires an average cooling rate of about 12°C m.y.$^{-1}$ during this time period (Figure 7), and the oldest ages in the spectrum suggest closure through 375°C at about 14 Ma and are consistent with the coexisting muscovite age of 14.2 Ma.

Lower Plate Cooling History

Northwest Part of Bare Mountain

A temperature-time curve constructed from lower plate thermochronologic data (Table 2) is given in figure 6 for the northwest part of Bare Mountain. The data indicate that rocks cooled slowly through 350±50° to 300±50°C between about 57 and 38 Ma, then cooled rapidly from 205±50° to 120±50°C between 12.6±1.6 and 11.1±1.9 Ma. This thermal history is consistent with the two K-feldspar $^{40}Ar/^{39}Ar$ MDD models (Figure 6) and consistent, within uncertainties, with the summary of apatite fission track data reported by Spivey et al. (1995).

It is possible to interpret the $^{40}Ar/^{39}Ar$ release spectra and conventional K-Ar data for muscovite and biotite as indicating rapid cooling in early Tertiary time, in contrast to the interpretation of slow cooling made above. Muscovite dates are older than biotite dates in three of four pairs listed in Table 2, the difference ranging from 10.4 to 3.5 m.y. Passage through muscovite and biotite closure temperatures in this range of times would indicate a cooling rate of ~10-20°C m.y.$^{-1}$ This cooling rate is highly sensitive to the difference in closure temperature of muscovite and biotite in each pair and could be much faster or slower depending upon the value. If cooling was rapid, all the dates on muscovite and biotite should be about the same, but this is not the case. The ages for both muscovite and biotite spread across about 16 Ma, reflective of slow cooling of micas having slightly different closure temperatures. Slow cooling (<5°C m.y.$^{-1}$) is supported by the age gradients in the mica $^{40}Ar/^{39}Ar$ age spectra (Figure 2) and the K-feldspar thermal histories (Figure 6). The most retentive portions of the K-feldspar samples are consistent with temperatures of ~300°C at ~25-30 Ma. Sustaining micas at temperatures near their bulk closure temperatures from ~30-60 Ma facilitates argon loss and development of a nonuniform argon concentration distribution and magnifies the effect of small differences in mineral closure temperatures.

The 60 Ma U-Pb apatite age determined from sample BM-TH-14ab might be regarded as too young compared to the K-Ar and $^{40}Ar/^{39}Ar$ mica ages of 57 to 38 Ma, considering the slow inferred cooling rate and the higher closure temperature of

apatite. For a scenario whereby rocks cooled at a constant rate from a peak temperature of ~530°C at 130 Ma down to ~200°C at 15 Ma, the apatite would have passed below 475±50°C at ~110 Ma. Possible explanations of the discrepancy include (1) uncertainty in the blocking temperature of apatite, (2) delayed cooling following peak metamorphism, and (3) Pb isotopic disequilibrium between apatite and plagioclase. The latter possibility is particularly intriguing because plagioclase remains open to Pb exchange, perhaps down to 200°C, after closure of apatite. Radiogenic Pb acquired by the plagioclase after apatite closure would reduce the difference in isotopic composition between the two minerals, causing a reduction in the apparent age of the apatite. The 60 Ma age calculated on the basis of isotopic equilibrium is therefore accepted only as a minimum.

The cooling history (Figure 6) suggests that unroofing took place slowly through early Tertiary time and that the rocks were at a temperature of ~250°C just prior to the onset of rapid cooling at about 12.7 Ma. The 250°C estimate is just above the annealing temperature for fission tracks in zircon and is consistent with the two K-feldspar $^{40}Ar/^{39}Ar$ MDD models which indicate a temperature of 275±40°C. This temperature equates to a depth of 8-10 km if the inferred Cretaceous geothermal gradient of 27°C km^{-1} [*Hoisch*, 1997] was maintained through early and mid-Tertiary time. It is possible that Tertiary volcanism in the region raised the geothermal gradient just prior to the onset of detachment faulting; however, the paucity of Tertiary dikes in the lower plate suggests a lack of proximity to major magma conduits, consistent with the main volcanic centers being located about 20 km to the east. There was also insufficient time for large-scale heating of the crust to have taken place in response to the passage of 14.0-11.45 Ma magmas associated with the major volcanic centers.

Bullfrog Hills

A temperature-time curve constructed from thermochronologic data (Table 2) from the lower plate of the Bullfrog Hills is given in figure 7. The data indicate that the lower plate cooled slowly through 500±50°C at about 78 Ma, passed through 350±50° to 300±50°C between 16.3±0.4 and 10.5±0.3 Ma, and then cooled rapidly from 285±50° to 120±50°C between 8.9±1.4 and 10.6±2.0 Ma. For the last interval, the youngest age corresponds to the highest closure temperature, and thus all three fission track minerals underwent closure at about the same time. The overlap of the 2σ error brackets for all five fission track dates may therefore be considered a better indication of the cooling age: 10.2 Ma to 8.6 Ma. Two of the five fission track dates fall outside this interval, but their 2σ error brackets fall within it. The thermal history derived from the K-feldspar $^{40}Ar/^{39}Ar$ data (BF-MO-5c) indicates that rapid cooling began at about 9-10 Ma, which is in excellent agreement the rest of the thermochronologic data (Figure 7b).

Similar to northwest Bare Mountain, tilting in the upper plate between 10.7 and 8.1 Ma was coeval with rapid cooling in the lower plate between 10.2 Ma to 8.6 Ma. The cooling history (Figure 7) suggests that lower plate rocks were denuded slowly through the Late Cretaceous and early Tertiary and was at a depth of about 15±2 km just prior to rapid cooling. The depth estimate was arrived at by considering a temperature of 400±50°C (just above the Ar closure temperature of biotite) divided by the Cretaceous geothermal gradient of 27°C km^{-1} determined by *Hoisch* [1997], although, as discussed previously with reference to the northwest part of Bare Mountain, the geothermal gradient might have been higher just prior to detachment faulting.
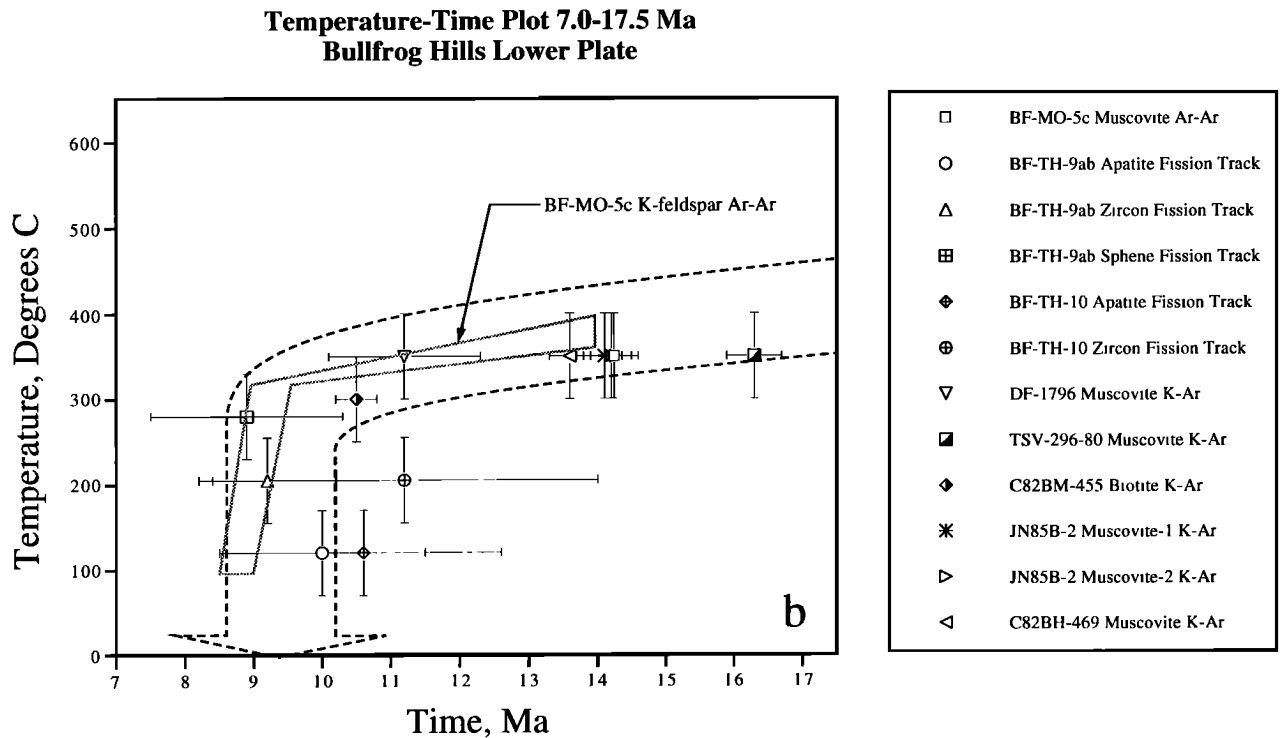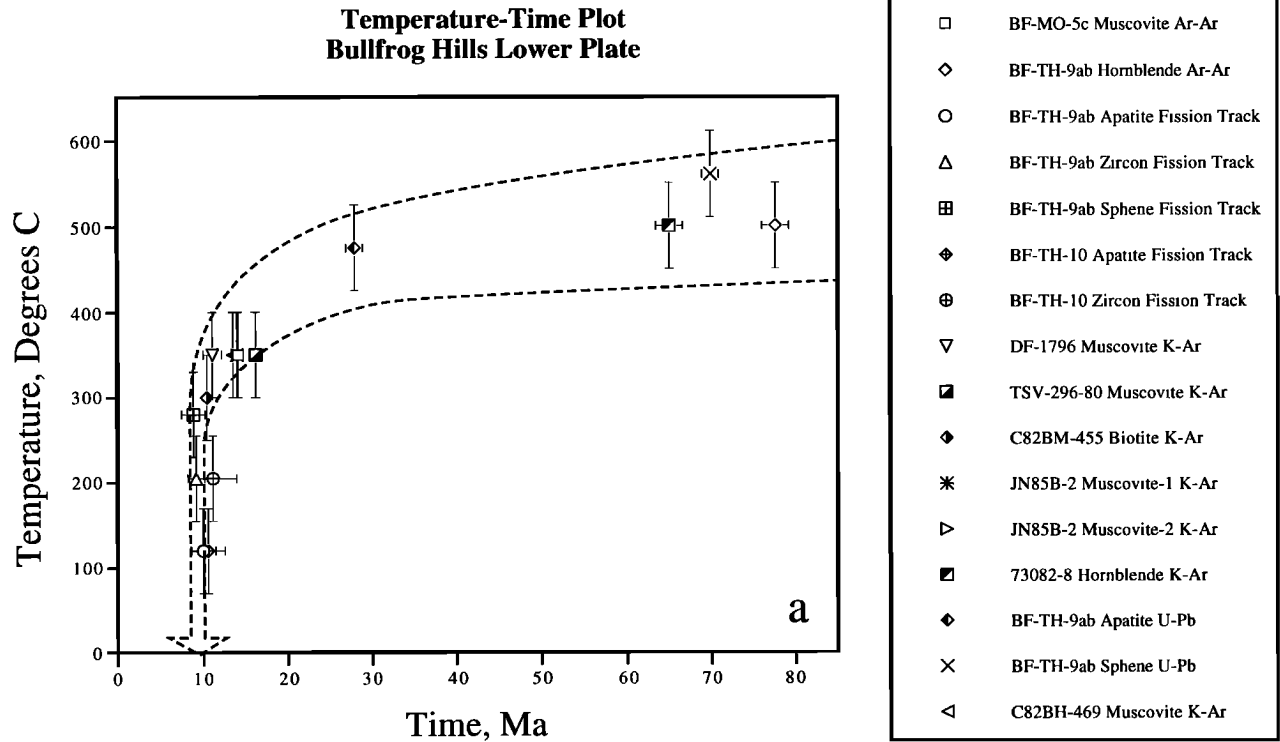
Figure 7. Temperature-time plots for lower plate rocks from the Bullfrog Hills, based on data reported in Table 2. Dashed arrow shows inferred temperature-time path. (a) All cooling ages except for the MDD model of the K-feldspar Ar-Ar data for BF-MO-5c. (b) Expanded diagram for cooling ages between 7.0 Ma and 17.5 Ma and including the K-feldspar MDD model of the K-feldspar Ar-Ar data. The K-feldspar thermal history window represents uncertainty in the age spectrum and diffusion domain distribution. The absolute temperature value for the thermal history is most sensitive to the choice of the activation energy and thus could shift up or down the y axis by ~40°C to accommodate the uncertainty in activation energy.
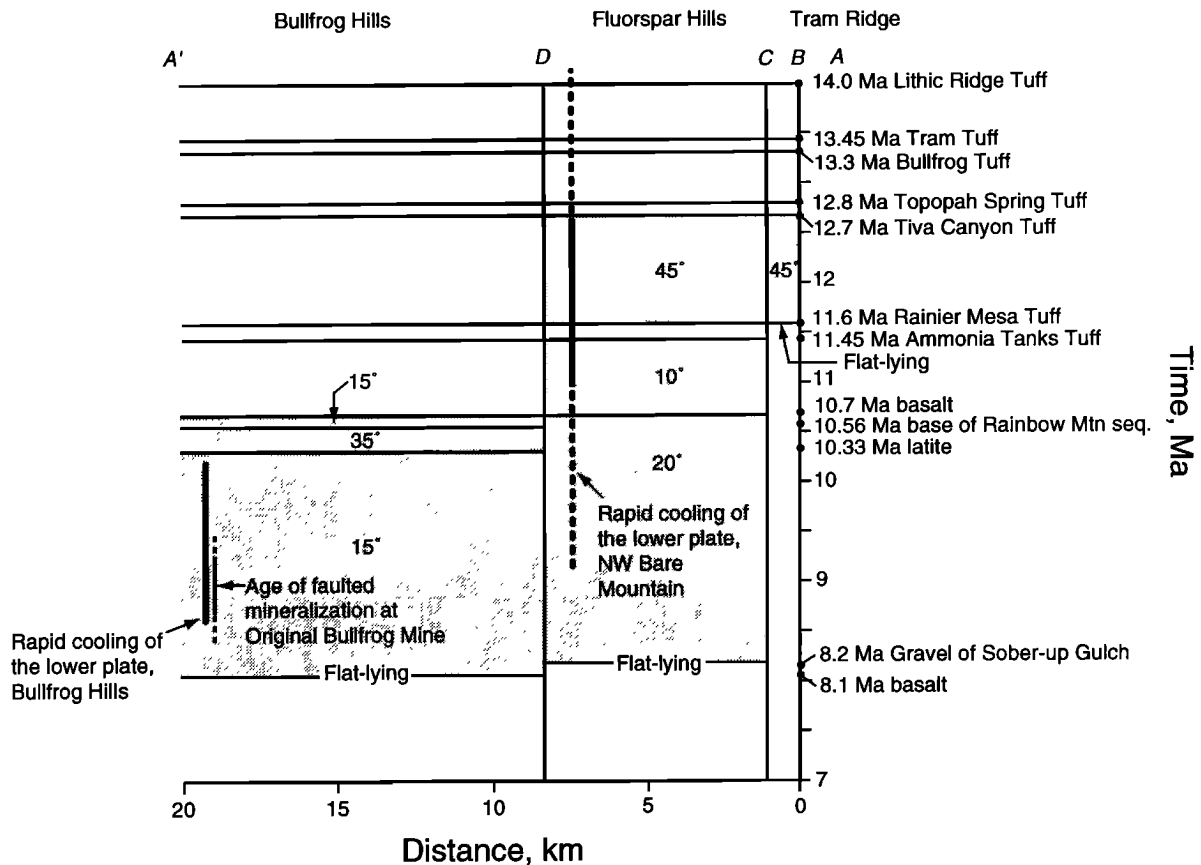
Figure 8. Angular unconformities (shaded intervals) placed in time and space across upper plate transect A-A' (Figure 1). Angles shown are approximate (±10°). Faults B (west flank of Tram Ridge), C, and D delineate different domains. Periods of rapid lower plate cooling (uplift), projected onto the transect, are also shown. The oldest flat-lying unit (±10°) in each domain is labeled. Upper plate relationships are based on work by Eng et al. [1996], Fridrich [1997], Maldonado [1990a,b], Maldonado and Hausback [1990], Monsen et al. [1992], and Weiss [1996].

Northwest Funeral Mountains

Rocks in the lower plate of the Boundary Canyon fault from the northwest part of the Funeral Mountains have been extensively dated in previous studies. The data indicate slow cooling from the peak of metamorphism (~700°C) in Early Cretaceous time through 500±50°C at ~70 Ma and through 300±50°C at 15 Ma, based on $^{40}Ar/^{39}Ar$ and K-Ar data on hornblende, muscovite and biotite [Applegate, 1994; Applegate et al., 1992; DeWitt et al., 1988; Hoisch and Simpson, 1993). This was followed by rapid cooling from 285±50° to 120±50 °C between 10.6±1.6 and 5.6±1.4 Ma, based on fission track data on sphene, zircon, and apatite [Holm and Dokka, 1991; Hoisch and Simpson, 1993]. The cooling history is broadly similar to lower plate rocks in the Bullfrog Hills. The potential may exist to date movement along the Boundary Canyon fault more precisely by examining relationships in the upper plate, but these have not yet been mapped in detail.

Discussion

In the Bullfrog Hills and Fluorspar Hills, tilting in the upper plate and rapid cooling in the lower plate underwent an east-southeast to west-northwest progression across ~20 km (Figure 8). The difference in the age of upper plate tilting between the two areas is accurately elucidated from the analysis of angular unconformities, however, the rapid cooling portions of the lower plate cooling histories partially overlap within uncertainties. Both the initiation and cessation of tilting in the upper plate underwent west-northwest migration (Figure 8).

Faulting along the breakaway of the detachment began before 12.7 Ma. Tilting in the hanging wall of the breakaway took place from 12.7 Ma to 11.6 Ma and was over by 11.6 Ma. In the central and western Fluorspar Hills, tilting took place from 12.7 Ma to 10.7 Ma, continued less strongly after 10.7 Ma and was over by 8.2 Ma. The maximum time interval over which tilting may have occurred is 4.5 Ma, from 12.7 to 8.2 Ma, and the minimum is 0.9 Ma, from 11.6 to 10.7 Ma (Figure 8). Considering that there was 9±2 km of denudation of the lower plate in the in the northwest part of Bare Mountain, minimum and maximum uplift rates are calculated to be 2.0±0.4 and 10±2 mm yr⁻¹, respectively. In the Bullfrog Hills upper plate, tilting took place between 10.7 Ma and 10.3 Ma, continued less strongly after 10.3 Ma, and was over by 8.1 Ma. The lower plate rose 15±2 km within a maximum possible interval of 2.6 m.y., from 10.7 to 8.1 Ma (Figure 8), which indicates a minimum uplift rate of 6±1 mm yr⁻¹.

The midpoints of the time intervals for rapid tilting in the upper plate are 12.15 Ma near the breakaway at Tram Ridge (12.7-11.6 Ma) and 10.5 Ma (10.7-10.3 Ma) in the Bullfrog Hills. Thus, it took about 1.65 m.y. for the locus of rapid tilting to

migrate west-northwest across a horizontal distance of about 20 km, which indicates a migration rate of 12 mm yr^{-1}. The west-northwest migration of rapid tilting may be related to the migration of the hinge of the detachment fault.

The thermochronologic data (summarized in Table 2 and Figures 6 and 7) indicate that the lower plate in the Bullfrog Hills and at Bare Mountain cooled slowly through the Late Cretaceous and much of the Tertiary. Slow cooling is consistent with a slow rate of denudation related to surface erosion. Erosion during this period is suggested by the lack of Cretaceous and early Tertiary sediments within a broad region that includes the study area. It is also consistent with the development of extensive thrust belts in the region in Mesozoic time, which should have produced a thickened crust and high elevations. Erosion probably stripped Bare Mountain down to the 225°C Cretaceous isotherm (8-9 km of erosion assuming the Cretaceous geothermal gradient of 27°C km^{-1} of *Hoisch* [*1997*], as indicated by the lowest value of conodont color alteration indexes (4.0) obtained from exposed Paleozoic rocks at Bare Mountain [*Grow et al.*, 1994].

The lower plate of the Bullfrog Hills experienced a greater amount of denudation associated with detachment faulting (15±2 km) than the lower plate in the northwest part of Bare Mountain (9±2 km). The increase in denudation to the west-northwest implies a west-northwestward dip to the detachment fault surface. The fault cut downward from the upper Proterozoic and Paleozoic strata exposed at Bare Mountain, through ~5000 m of unexposed Late Proterozoic strata, to the 1.7 Ga basement rocks exposed in the Bullfrog Hills. Before detachment faulting began, the lower plate rocks at Bare Mountain had already cooled below 300°C, while the lower plate rocks in the Bullfrog Hills were still above 300°C. Thus the subsequent lower plate response to detachment faulting was brittle at Bare Mountain and ductile (mylonitic) in the Bullfrog Hills. A limit may be placed on the dip angle of the fault. The thermochronologic sample areas are separated by a horizontal distance of about 12 km (Figure 1). The inferred difference in depth at the time of fault initiation is ~6 km. Simple triangulation indicates a dip of ~30°, which represents the cumulative rotation of both the fault and lower plate. If the lower plate underwent extension during the process, which seems likely, then the horizontal distance was less than 12 km and the dip angle greater than 30°. The large uncertainties associated with the values used in this calculation limit the dip angle only insofar as suggesting that it was moderate and that it was unlikely to have been very gentle or very steep.

An original fault dip of west-northwest is suggested by west-northwest movement along normal faults in the upper plate, west-northwest shear in lower plate mylonites in the Bullfrog Hills, and the differential depth of the lower plate at the time rapid cooling began. The present-day orientation of the fault differs; at the surface, the Fluorspar Canyon fault currently dips moderately to the north and the Bullfrog segment probably dips gently to the north (discussed previously). Fault rotation has removed the dominant westerly component of the original dip.

At Bare Mountain, the lower plate may have responded to denudation by movement along the east dipping normal faults. Movement along these faults exposed deeper crustal levels westward, consistent with conodont color alteration index data [*Grow et al.*, 1994] and metamorphic petrology [*Hoisch*, 1997]. The normal faults in the lower plate were active between 16.9 and 8.2 Ma, which is permissive of movement during upper plate normal faulting (12.7 to 8.2 Ma) and rapid cooling of lower plate rocks in the northwest part of Bare Mountain (12.6±1.6 to 11.1±1.9 Ma).

The data allow for a discontinuous migration of activity in the upper plate, in which domains of normal faulting and tilting (Figure 8) stepped west-northwest when new breakaways developed in the detachment. The findings permit the rolling hinge model of detachment faulting proposed by *Hamilton* [1988a, 1988b] for this area, but do not uniquely determine it. Along the Bullfrog segment of the detachment, the occurrence of slivers of Paleozoic subgreenschist facies rocks between the upper and lower plates suggests that the process involved incising pieces from the lower plate and dragging them along the fault. Multiple detachments, such as proposed by *Maldonado* [1990b], offer an alternative explanation.

Appendix

The ^{40}Ar/^{39}Ar data taken in this study are available as an electronic supplement. The supplement contains three data tables. Table A1 includes the data for muscovite, biotite, and hornblende. Table A2 includes data for K-feldspar. Table A3 includes multigrain laser fusion data for muscovite.

References

Applegate, J.D.R., The unroofing history of the Funeral Mountains metamorphic core complex, California, Ph.D. thesis, Mass. Inst. of Technol., Cambridge, 1994.

Applegate, J.D.R., J.D. Walker, and K.V. Hodges, Late Cretaceous extensional unroofing in the Funeral Mountains metamorphic core complex, *Geology, 20,* 519-522, 1992.

Axen, G.J., Pore pressure, stress increase, and fault weakening in low-angle normal faulting, *J. Geophys. Res., 97,* 8979-8991, 1992.

Axen, G.J., Ramp-flat detachment faulting and low-angle normal reactivation of the Tule Springs thrust, southern Nevada, *Geol. Soc. Am. Bull., 105,* 1076-1090, 1993.

Axen, G.J., and J. Selverstone, Stress state and fluid-pressure level along the Whipple detachment fault, California, *Geology, 22,* 835-838, 1994.

Axen, G.J., J.M. Bartley, and J. Selverstone, Structural expression of a rolling hinge in the footwall of the Brenner Line normal fault, eastern Alps, *Tectonics, 14,* 1380-1392, 1995.

Bartley, J.M., J.M. Fletcher, and A F. Glazner, Tertiary extension and contraction of lower-plate rocks in the central Mojave metamorphic core complex, southern California, *Tectonics, 9,* 521-534, 1990.

Brun, J.-P., D. Sokoutis, and J. van den Driessche, Analogue modeling of detachment systems and core complexes, *Geology, 22,* 319-322, 1994.

Buck, W.R., Flexural rotation of normal faults, *Tectonics, 7,* 959-973, 1988.

Buck, W.R., Effect of lithospheric thickness of the formation of high- and low-angle normal faults, *Geology, 21,* 933-936, 1993.

Burgess, R., and I. Parsons, Argon and halogen geochemistry of hydrothermal fluids in the Lock Ainort granite, Isle of Skye, Scotland, *Contrib. Mineral. Petrol, 115,* 345-355, 1994.

Burgess, R., S.P. Kelley, I. Parsons, F.D.L. Walker, and R.H. Worden, ^{40}Ar-^{39}Ar analysis of perthite microstructures and fluid inclusions in alkali feldspars from the Klokken syenite, South Greenland, *Earth. Planet. Sci. Lett., 109,* 147-167, 1992.

Byers, F.M., Jr., W.J. Carr, P.P. Orkild, W.D. Quinlivan, and K.A. Sargent, Volcanic suites and related cauldrons of the Timber Mountain–Oasis Valley caldera complex, southern Nevada, *U.S. Geol. Surv. Prof. Pap., 919,* 70 pp., 1976.

Carr, M.D., and S.A. Monsen, A field trip guide to the geology of Bare Mountain, in *This Extended Land–Geological Journeys in the Southern Basin and Range*, edited by D.L. Weide and M.L. Faber, *Spec. Publ. 2*, pp. 50-57, Univ. of Nev. Geosci. Dep., Las Vegas, 1988.

Carr, W.J., Regional structural setting of Yucca Mountain, southwestern Nevada, and Late Cenozoic rates of tectonic activity in part of the southwestern Great Basin, Nevada and California, *U.S. Geol. Surv. Open File Rep., 84-854*, 109 pp., 1984.

Carr, W.J., Volcano-tectonic setting of Yucca Mountain and Crater Flat, southwestern Nevada, *U.S. Geol. Surv. Bull., 1790*, 35-49, 1988.

Carr, W.J., Styles of extension in the Nevada Test Site region, southern Walker Lane belt; an integration of volcano-tectonic and detachment fault models, in *Basin and Range Extensional Tectonics near the Latitude of Las Vegas, Nevada*, edited by B.P. Wernicke, *Mem. Geol. Soc. Am., 176*, 283-303, 1990.

Carr, W.J., and L.D. Parrish, Geology of drill hole VH-2, and structure of Crater Flat, southwestern Nevada, *U.S. Geol. Surv. Open File Rep., 85-475*, 41 pp., 1985.

Carr, W.J., F.M. Byers, Jr., and P.P. Orkild, Stratigraphic and volcano-tectonic relations of the Crater Flat Tuff and some older volcanic units, *U.S. Geol. Surv. Prof. Pap., 1323*, 28 pp., 1986.

Cherniak, D.J., Lead diffusion in titanite and preliminary results on the effects of radiation damage on Pb transport, *Chem. Geol., 110*, 177-194, 1993.

Cherniak, D.J., W.A. Lanford, and F.J. Ryerson, Lead diffusion in apatite and zircon using ion implantation and Rutherford backscattering techniques, *Geochim. Cosmochim. Acta, 55*, 1663-1674, 1991.

Coleman, D.S., and D.J. Walker, Modes of tilting in extensional core complex development, *Science, 263*, 215-218, 1994.

Conners, K.A., S.I. Weiss, and D.C. Noble, The Oasis Valley Fault–The principal breakaway structure and eastern limit of Late Miocene syn-volcanic extension in the Bullfrog Hills, southwestern Nevada (abstract), *Eos Trans. AGU, 76 (17)*, Spring Meet. Suppl., S284, 1995.

Cornwall, H.R., and F.J. Kleinhampl, Geology of the Bare Mountain Quadrangle, scale 1:62,500, *U.S. Geol. Surv. Map, GQ-157*, 1961.

Crittenden, M.D., P.J. Coney, and G.H . Davis, Cordilleran metamorphic core complexes, *Mem. Geol. Soc. Am., 153*, 4-34, 1980.

Davis, G.A., and G.S. Lister, Detachment faulting in continental extension; Perspectives from the southwestern U.S. Cordillera, in *Processes in Continental Lithospheric Deformation*, edited by S.P. Clark Jr., B.C. Burchfiel, and J. Suppe, *Spec. Pap. Geol. Soc. Am. 218*, 133-160, 1988.

Davis, G.H., Shear zone model for the origin of metamorphic core complexes, *Geology, 11*, 342-347, 1983.

Davis, G.H., A shear zone model for the structural evolution of metamorphic core complexes in southeastern Arizona, in *Continental Extensional Tectonics*, edited by M.P. Coward, J.F. Dewey, and P.L. Hancock, *Geol. Soc. Spec. Publ. 28*, 247-266, 1987.

Davis, G.H., and P.J. Coney, Geological development of metamorphic core complexes, *Geology, 7*, 120-124, 1979.

Deino, A.L., B.P. Hausback, B.T Turrin, and E.H. McKee, New ^{40}Ar/^{39}Ar ages for the Spearhead and Civet Cat Members of the Stonewall Flat Tuff, Nye County, Nevada (abstract), *Eos Trans. AGU, 70*, 1409, 1989.

DeWitt, E.J., J.E. Sutter, L.A. Wright, and B.W. Troxel, Ar-Ar chronology of Early Cretaceous regional metamorphism, Funeral Mountains, California–A case study of excess argon (abstract), *Geol. Soc. Am. Abstr. Programs, 20*, 16, 1988.

Dokka, R.K., M.J. Mahaffe, and A.W. Snoke, Thermochronologic evidence of major tectonic denudation associated with detachment faulting, northern Ruby Mountains, East-Humbolt Range, Nevada, *Tectonics, 5*, 995-1006, 1986.

Eng, T., D.R. Boden, M.R. Reischman, and J.O. Biggs, Geology and mineralization of the Bullfrog Mine and vicinity, Nye County, Nevada, in *Geology and Ore Deposits of the American Cordillera, Symposium Proceedings*, edited by A.R. Coyner and P.L. Fabey, pp. 353-402, Geol. Soc. of Nev., Reno, 1996.

Faulds, J.E., J.W. Bell, D.L. Feuerbach, and A.R. Ramelli, Geologic map of the Crater Flat area, Nevada, scale 1:24,000, *Nev. Bur. Mines Geol. Map, 101*, 1994.

FitzGerald, J.D., and T.M. Harrison, Argon diffusion domains in K-feldspar, I, Microstructures in MH-10, *Contrib. Mineral. Petrol., 113*, 367-380, 1993

Foland, K.A., Argon diffusion in feldspars, in *Feldspars and Their*

Reactions, edited by L. Parsons, pp. 415-447, Kluwer Acad., Norwell, Mass., 1994.

Foster, D.A., A.J.W. Gleadow, S.J. Reynolds, and P.G. Fitzgerald, Denudation of metamorphic core complexes and the reconstruction of the transition zone, west central Arizona: Constraints from apatite fission track thermochronology, *J. Geophys. Res., 98*, 2167-2185, 1993.

Fridrich, C.J., Tectonic evolution of the Crater Flat Basin, in *Cenozoic Basins of the Death Valley Region*, edited by L.A. Wright and B.W. Troxel, *Spec. Pap. Geol. Soc. Am.*, in press, 1997.

Fridrich, C.J., Whitney, J.W., Hudson, M.R., and B.M. Crowe, Late Cenozoic extension, vertical-axis rotation, and volcanism in the Crater Flat basin, southwest Nevada, in *Cenozoic Basins of the Death Valley Region*, edited by L.A. Wright and B.W. Troxel, *Spec. Pap. Geol. Soc. Am.*, in press, 1997.

Frizzell, V.A., Jr., and J. Shulters, Geologic map of the Nevada Test Site, southern Nevada, scale 1:100,000, *U.S. Geol. Surv. Misc. Invest. Ser. Map, I-2046*, 1990.

Gascoyne, M., Evidence for the stability of the potential nuclear waste host, sphene, over geological time, from uranium-lead ages and uranium series disequilibrium measurements, *Appl. Geochem., 1*, 199-210, 1986.

Greybeck, J.D., and A.B. Wallace, Gold mineralization at Fluorspar Canyon near Beatty, Nye County, Nevada, in *Geology and Ore Deposits of the Great Basin, Symposium Proceedings*, edited by G.L. Raines, R.E. Lisle, R.W. Shafer, and W.W. Wilkenson, pp. 935-946, Geol. Soc. of Nev., Reno, 1991.

Grow, J.A., C.E. Barker, and A.G. Harris, Oil and gas exploration near Yucca Mountain, southern Nevada, *Proc. Am. Nucl. Soc., 3*, 1298-1315, 1994.

Hamilton, W.B., Detachment faulting in the Death Valley region, California and Nevada, *U.S. Geol. Surv. Bull., 1790*, 51-85, 1988a.

Hamilton, W.B., Death Valley tectonics–Hingeline between active and inactivated parts of a rising and flattening master normal fault, in *Geology of the Death Valley Region, Field Trip Guideb.* vol. 16, edited by J.L. Gregory, and E.J. Baldwin, pp. 179-205, South Coast Geol. Soc., Santa Ana, Calif., 1988b.

Harrison, T.M., R.L. Armstrong, C.W. Naeser, and J.E. Harakal, Geochronology and thermal history of the coast plutonic complex, near Prince Rupert, British Columbia, *Can. J. Earth Sci., 16*, 400-410, 1979.

Harrison, T.M., W. Chen, P.H. Leloup, F.J. Ryerson,and P. Tapponier, An early Miocene transition in deformation regime within the Red River Fault Zone, Yunnan, and its significance for Indo-Asian tectonics, *J. Geophys. Res., 97*, 7159-7182, 1992.

Harrison, T.M., M.T. Heizler, and O.M. Lovera, In vacuo crushing experiments and K-feldspar thermochronometry, *Earth Planet. Sci. Lett., 117*, 169-180, 1993.

Harrison, T.M., M.T. Heizler, O.M. Lovera, W. Chen, and M. Grove, A chlorine disinfectant for excess argon released from K-feldspar during step heating, *Earth Planet. Sci. Lett., 123*, 95-104, 1994.

Heizler, M.T., and T.M. Harrison, K-feldspar ^{40}Ar/^{39}Ar constraints on the thermal history of New York (abstract), *Eos, Trans. AGU, 73 (43)*, Fall Meet. Suppl. 653, 1992.

Heizler, M.T., D.R. Lux, and E.R. Decker, The age and cooling history of the Chain of Ponds and Big Island Pond plutons and the Spider Lake granite, west-central Maine and Quebec, *Am. J. Sci., 288*, 925-952, 1988.

Hoisch, T.D., Conditions of metamorphism in lower-plate rocks at Bare Mountain, Nevada: Implications for extensional faulting, in *Tectonic Characterization of Yucca Mountain--a Potential Geologic Repository for Nuclear Wastes*, edited by J. Whitney, Spec. Pap. Geol. Soc. Am., in press, 1997.

Hoisch, T.D., and C. Simpson, Rise and tilt of metamorphic rocks in the lower plate of a detachment fault in the Funeral Mountains, Death Valley, California. *J. Geophys. Res., 98*, 6805-6827, 1993.

Holm, D.K., and D.K. Dokka, Major late Miocene cooling of the middle crust associated with extensional orogenesis in the Funeral Mountains, California, *Geophys. Res. Lett., 18*, 1775-1778, 1991,

Holm, D.K , and D.K. Dokka, Interpretation and tectonic implications of cooling histories: An example from the Black Mountains, Death Valley extended terrane, California, *Earth Planet. Sci. Lett., 116*, 63-80, 1993.

Holm, D.K., and B. Wernicke, Black Mountains crustal section, Death Valley extended terrain, California, *Geology, 18*, 520-523, 1992.

Holm, D.K., J.K. Snow, and D.R. Lux, Thermal and barometric constraints on the intrusion and unroofing history of the Black Mountains: Implications for timing, initial dip, and kinematics of detachment faulting in the Death Valley region, *Tectonics, 11*, 507-522, 1992.

Jackson, J.A., Active normal faulting and crustal extension, in *Continental Extensional Tectonics*, edited by M.P. Coward, J.F. Dewey, and P.L. Hancock, *Geol. Soc. Spec. Publ. 28*, pp. 3-17, 1987.

John, B.J., and D.A. Foster, Structural and thermal constraints on the initiation angle of detachment faulting in the southern Basin and Range: The Chemehuevi Mountains case study, *Geol. Soc. Am. Bull. 105*, 1091-1108, 1993.

King, G., and M. Ellis, The origin of large local uplift in extensional regions, *Nature, 348*, 689-693, 1990.

Klinger, R.E., and L.W. Anderson, Topographic profiles and their implications for Late Quaternary activity on the Bare Mountain fault, Nye County, Nevada (abstract), *Geol. Soc. Am. Abstr. Programs, 26*, 63-64, 1994.

Labotka, T.C., Petrology of a medium-pressure regional metamorphic terrane, Funeral Mountains, California, *Am. Mineral., 65*, 670-689, 1980.

Lee, J., Rapid uplift and rotation of mylonitic rocks from beneath a detachment fault: Insights from potassium feldspar $^{40}Ar/^{39}Ar$ thermochronology, northern Snake Range, Nevada: *Tectonics, 14*, 54-77, 1995.

Leloup, P.H., T.M. Harrison, F.J. Ryerson, Chen W., Li Q., P. Tapponnier, and R. Lacassin, Structural, petrological and thermal evolution of a Tertiary ductile strike-slip shear zone, Diancang Shan, Yunnan, *J. Geophys. Res, 98*, 6715-6743, 1993.

Livacarri, R.F., J.W. Geissman, and S.J. Reynolds, Paleomagnetic evidence for large-magnitude low-angle normal faulting in a metamorphic core complex, *Nature, 361*, 56-59, 1993.

Livacarri, R.F., J.W. Geissman, and S.J. Reynolds, Large-magnitude extensional deformation in the South Mountains metamorphic core complex, Arizona: Evaluation with paleomagnetism, *Geol. Soc. Am. Bull, 107*, 877-894, 1995.

Lovera, O.M., F.M. Richter, and T.M. Harrison, The $^{40}Ar/^{39}Ar$ thermochronology method for slowly cooled samples having a distribution of diffusion domain sizes, *J. Geophys. Res., 94*, 17917-17935, 1989.

Lovera, O.M., F.M. Richter, and T.M. Harrison, Diffusion domains determined by ^{39}Ar releases during step heating, *J. Geophys. Res., 96*, 2057-2069, 1991.

Lovera, O.M., M.T. Heizler, and T.M. Harrison, Argon diffusion domains in K-feldspar, II, Kinetic properties of MH-10 K-feldspar, *Contrib. Mineral. Petrol., 113*, 381-393, 1993.

Maldonado, F., Geologic map of the northwest quarter of the Bullfrog 15-minute quadrangle, Nye County, Nevada, scale 1:24,000, *U.S. Geol. Surv. Misc. Invest. Ser. Map, I-1985*, 1990a.

Maldonado, F., Structural geology of the upper plate of the Bullfrog Hills detachment fault system, southern Nevada, *Geol. Soc. Am. Bull., 102*, 992-1006, 1990b.

Maldonado, F., and B.P. Hausback, Geologic map of the northeast quarter of the Bullfrog 15-minute quadrangle, Nye County, Nevada, scale 1:24,000, *U.S. Geol. Surv. Misc. Invest. Map, I-2049*, 1990.

Manning, A.H., and J.M. Bartley, Postmylonitic deformation in the Raft River metamorphic core complex, northwestern Utah: Evidence of a rolling hinge, *Tectonics, 13*, 596, 1994.

Marvin, R.F., and J.C. Cole, Radiometric ages–Compilation A, U.S. Geological Survey, *Isochron West, 22*, 3-14, 1978.

Marvin, R.F., H.H. Mehnert, and C.W. Naeser, U.S Geological Survey radiometric ages–Compilation "C" part three–California and Nevada, *Isochron West, 52*, 3-11, 1989.

McDougall, I., and T.M. Harrison, *Geochronology and Thermochronology by the $^{40}Ar/^{39}Ar$ Method*, Oxford Univ. Press, New York, 1988.

McGrew, A.J., and L.W. Snee, $^{40}Ar/^{39}Ar$ thermochronologic constraints on the tectonothermal evolution of the northern East Humbolt Range metamorphic core complex, Nevada, *Tectonophysics, 238*, 425-450, 1994.

McIntosh, W.C., and S.M. Cathers, $^{40}Ar/^{39}Ar$ geochronology of basaltic rocks and constraints on the late Cenozoic stratigraphy and landscape development in the Red Hill-Quemado area, New Mexico, in *Mogollon Slope, West-Central New Mexico and East-Central Arizona, Field Conf. Guideb. N.M. Geol. Soc., 45th*, 209-224, 1994.

McKee, E.H., Reset K-Ar ages–Evidence for three metamorphic core complexes, western Nevada, *Isochron West, 38*, 17-20, 1983.

McKee, E.H., and J.R. Bergquist, New radiometric ages related to alteration and mineralization in the vicinity of Yucca Mountain, Nye County, Nevada, *U.S. Geol. Surv. Open File Rep., 93-538*, 26 pp., 1993.

Melosh, H.J., Mechanical basis for low-angle normal faulting in the Basin and Range province, *Nature, 343*, 331-335, 1990.

Miller, J.M.G., and B.J. John, Detachment strata in a Tertiary low-angle fault terrane, southeastern California: A sedimentary record of unroofing, breaching, and continued slip, *Geology, 16*, 645-648, 1988.

Miller, M.G., High-angle origin of the currently low-angle Badwater Turtleback fault, Death Valley, California, *Geology, 19*, 72-375, 1991.

Minor, S.A. and R.J. Fleck, Miocene landsliding and extensional faulting in the upper plate of the Bullfrog Hills detachment fault system, northern Bullfrog Hills, southern Nevada (abstract), *Geol. Soc. Am. Abstr. Programs, 26*, 75, 1994.

Monsen, S.A., M.D. Carr, M.C. Reheis, and P.P. Orkild, Geologic map of Bare Mountain, Nye County, Nevada, scale 1:24,000, *U.S. Geol. Surv. Misc. Invest. Ser. Map, I-2201*, 1992.

Morton, J.L., M.L. Silberman, H.F. Bonham, L.J. Garside, and D.C. Noble, K-Ar ages of volcanic rocks, plutonic rocks, and ore deposits in Nevada and eastern California–Determinations run under the USGS-NBMG cooperative program, *Isochron West, 20*, 19-29, 1977.

Noble, D.C., S.I. Weiss, and E.H. McKee, Magmatic and hydrothermal activity, caldera geology, and regional extension in the western part of southwestern Nevada volcanic field, in *Geology and Ore Deposits of the Great Basin*, edited by G.L. Raines, R.E. Lisle, R.W. Shafer, and W.W. Wilkenson, pp. 913-934, Geol. Soc. of Nev., Reno, 1991.

Parsons, I., D.C. Rex, P. Guise, and A.N. Haliday, Argon-loss by alkali feldspars, *Geochim. Cosmochim. Acta, 52*, 1097-1112, 1988.

Ransome, F.L., W.H. Emmons, and G.H. Gary, Geology and ore deposits of the Bullfrog District, Nevada, *U.S. Geol. Surv. Bull., 125* pp., *407*, 1910.

Reheis, M.C., Preliminary study of Quaternary faulting on the east side of Bare Mountain, Nye County, Nevada, *U.S. Geol. Surv. Bull. 1790*, 103-111, 1988.

Reynolds, M.W., L.A. Wright, and B.W. Troxel, Geometry and chronology of Late Cenozoic detachment faulting, Funeral and Grapevine Mountains, Death Valley, California (abstract), *Geol. Soc. Am. Abstr. Programs, 18*, 175, 1986.

Richard, S.M., J.E. Fryxell, and J.F. Sutter, Tertiary structure and thermal history of the Harquahala and Buckskin Mountains, west central Arizona: Implications for denudation by a major detachment fault system, *J. Geophys. Res., 95*, 19973-19987, 1990.

Sawyer, D.A., R.J. Fleck, M.A. Lanphere, R.G. Warren, D.E. Broxten, and M.R. Hudson, Episodic caldera volcanism in the Miocene southwestern Nevada volcanic field–Revised stratigraphic framework, $^{40}Ar/^{39}Ar$ geochronology, and implications for magmatism and extension, *Geol. Soc. Am. Bull., 106*, 1304-1318, 1994.

Scott, R.J., and G.S. Lister, Detachment faults: Evidence for a low angle origin, *Geology, 20*, 833-836, 1992.

Selverstone, J., G.J. Axen, and J.M. Bartley, Fluid inclusion constraints on the kinematics of footwall uplift beneath the Brenner Line normal fault, eastern Alps, *Tectonics, 14*, 1076, 1995.

Spencer, J.E., and C.G. Chase, Role of crustal flexure in initiation of low-angle normal faults and implications for structural evolution of the Basin and Range province, *J. Geophys. Res., 94*, 1765-1775, 1989.

Spencer, J.E., and S.J. Reynolds, Tertiary structure, stratigraphy, and tectonics of the Buckskin Mountains, in *Geology and Mineral Resources of the Buckskin and Rawhide Mountains, West-Central Arizona*, edited by J.E. Spencer and S.J. Reynolds, *Bull. 198, pp.* 103-167, *Ariz. Geol. Soc.*, 1989.

Spencer, J.E., and S.J. Reynolds, Tectonics of mid-Tertiary extension along a transect through west central Arizona, *Tectonics, 10*, 1204-1221, 1991.

Spivey, K.H., D.A. Ferrill, and J. Stamatakos, Uplift and cooling history of Bare Mountain, Nevada, from apatite fission track thermochronology (abstract), *Geol. Soc. Am. Abstr. Programs, 27*, 389, 1995.

Swadley, W.C., and W.J. Carr, Geologic map of the Quaternary and Tertiary deposits of the Big Dune Quadrangle, Nye County, Nevada, and Inyo County, California, scale 1:48,000, *U.S. Geol. Surv. Misc. Invest. Ser. Map, I-1767*, 1978.

Turner, G., and S. Wang, Excess argon, crustal fluids and apparent isochrons from crushing K-feldspar, *Earth Planet. Sci. Lett., 110*, 193-211, 1992.

Wdowinski, S., and G.J. Axen, Isostatic rebound due to tectonic denudation: A viscous flow model of a layered lithosphere, *Tectonics, 11*, 303-315, 1992.

Weiss, S.I., Hydrothermal activity, epithermal mineralization, and regional extension in the southwestern Nevada volcanic field, Ph.D. thesis, Univ. of Nev., Reno, 1996.

Weiss, S.I., K.A. Conners, D.C. Noble, and E.H. McKee, Coeval extension and magmatic activity in the Bullfrog Hills, during the later phases of Timber Mountain volcanism (abstract), *Geol. Soc. Am. Abstr. Programs, 22*, 92-93, 1990.

Weiss, S.I., E.H. McKee, D.C. Noble, and K.A. Conners, Multiple episodes of Au-Ag mineralization in the Bullfrog Hills, SW Nevada, and their relation to coeval extension and volcanism (abstract), *Geol. Soc. Am. Abstr. Programs, 23*, 246, 1991.

Wernicke, B., Low-angle normal faults and seismicity: A review, *J. Geophys. Res., 100*, 20159-20174, 1995.

Wernicke, B., and G.J. Axen, On the role of isostacy in the evolution of normal fault systems, *Geology, 16*, 848-851, 1988.

Wernicke, B., P.L. Guth, and G.J. Axen, Tertiary extensional tectonics in the Sevier thrust belt of southern Nevada, in *Western Geological Excursions, Vol. 4*, edited by J. Lintz Jr., pp. 473-510, Geological Society of America and Department of Geological Sciences, Mackey School of Mines, University of Nevada, Reno, 1984.

West, D.P., Jr., and D.R. Lux, Dating mylonitic deformation by the ^{40}Ar-^{39}Ar method: An example from the Norumbega Fault Zone, Maine, *Earth Planet. Sci. Lett., 120*, 221-238, 1993.

Wright, L.A., and B.W. Troxel, Geologic map of the central and northern Funeral Mountains and adjacent areas, Death Valley region, southern California, scale 1:48,000, *U.S. Geol. Surv. Misc. Invest. Map, I-2305*, 1993.

Yin, A., Origin of regional, rooted, low-angle faults: A mechanical model and its tectonic implications, *Tectonics, 8*, 469-482, 1989.

Yin, A., and J.F. Dunn, Structural and stratigraphic development of the Whipple-Chemihuevi detachment fault system, southeast California: Implications for the geometrical evolution of domal and basinal low-angle normal faults, *Geol. Soc. Am. Bull., 104*, 659-674, 1992.

Zeitler, P.K., N.M. Johnson, C.W. Naeser, and R.A.K. Tahirkheli, Fission-track evidence for Quaternary uplift of the Nanga Parbat region, Pakistan, *Nature, 298*, 255-257, 1982.

M.T. Heizler, New Mexico Bureau of Mines and Mineral Resources, New Mexico Institute of Mining and Technology, Soccoro, NM 87801. (e-mail: matt@mailhost.nmt.edu)

T.D Hoisch, Department of Geology, Box 4099, Northern Arizona University, Flagstaff, AZ 86011. (e-mail: thomas.hoisch@nau.edu)

R.E. Zartman, Department of Geological Sciences, University of Cape Town, Rondebosch 7700, Republic of South Africa. (e-mail: rzart@geology.uct.ac.za)